mathematics

MDPI

Article

Source Inversion Based on Distributed Acoustic Sensing-Type Data

Litao Shen [1], Tian-Yi Wang [1,*] and Haoran Zhang [2]

[1] School of Science, Wuhan University of Technology, Wuhan 430070, China; vtao258@whut.edu.cn
[2] Department of Applied Mathematics, Hong Kong Polytechnic University, Hong Kong, China; mike-haoran.zhang@connect.polyu.hk
* Correspondence: tianyiwang@whut.edu.cn

Abstract: In this study, we investigate the inverse problem of the two-dimensional wave equation source term, which arises from the Distributed Acoustic Sensing (DAS) data on the boundary. We construct a new integral operator that maps the interior sources to the DAS-type data at the boundary. Due to the noninjectivity and instability of the integral operator, which violates the well posedness of the inverse problem, a minimization problem on a compact convex subset is formulated, and the existence and uniqueness of the minimizer are obtained. Numerical examples for different cases are illustrated.

Keywords: inverse problem; source term; DAS-type data

MSC: 35R30; 65M32; 65N21

1. Introduction

Distributed Acoustic Sensing (DAS) technology has received significant attention and application in the field of seismology [1], and with this has come the rapid development of fiber optic sensing technology. DAS technology relies on the Rayleigh scattering effect within the optical fiber to sense the local strain in the fiber that is caused by environmental vibrations in real time. Real-time, continuous, and distributed monitoring of the acoustic information of the surrounding environment is realized [2] using the scattering effect of the optical fiber for the detection and analysis of acoustic signals. It is known that DAS technology possesses significant advantages, such as continuous coverage, high sensitivity and low maintenance costs, as well as higher accuracy and robustness compared to point sensors [3]. As a cutting-edge new seismic signal acquisition technology, DAS has great potential and research value in the fields of pipeline monitoring, boundary intrusion monitoring, and oil and gas resource exploration [4].

The propagation of vibrations in a medium usually satisfies the wave equation, and the corresponding mathematical problem of inverting the shape and position of the vibrations source from the observed data is the inverse source problem of the wave equation, which has since attracted the attention of many researchers. Asiri, Zayane-Aissaa, and Laleg-Kirati in [5] developed an adaptive observer for the inverse source problem of a one-dimensional wave equation designed to estimate the state and source components of a fully discrete system. The effectiveness of the algorithm was verified in noise-free and noise-containing environments, and the effects of the measurement size and location on the results were analyzed. The inverted source term function was found to be time-independent. Shajari-Shidfar [6] examined the inverse source problem for wave equations with an overdetermination condition in the one-dimensional case, and they resolved it using the method of weighted homography analysis. To illustrate the accuracy and reliability of the proposed method, three numerical examples were given in the paper for verification. Hu-Kian-Zhao [7] investigated the inverse source problem with Dirichlet-kind dynamical

check for updates

Citation: Shen, L.; Wang, T.-Y.; Zhang, H. Source Inversion Based on Distributed Acoustic Sensing-Type Data. *Mathematics* **2024**, *12*, 1868. https://doi.org/10.3390/math12121868

Academic Editor: Andrea Scozzari

Received: 30 April 2024
Revised: 28 May 2024
Accepted: 4 June 2024
Published: 14 June 2024

boundary data in unbounded domains, and they proved uniqueness in recovering the source terms of form $f(x)g(t)$ and $f(x_1, x_2, t)h(x_3)$. Liu-Qiu-Wang [8] proposed a simple and efficient numerical technique based on the new idea of using homogenization functions to solve the nonlinear inverse wave source problem, where the aim was to accurately and quickly identify the wave source function without directly solving the nonlinear wave equation. Arumugam-Prakash-Nieto [9] explored the inverse problem of identifying a spacewise-dependent source term of the wave equation from boundary measurement data. The aforementioned paper transformed the inverse problem into an optimization problem based on the optimal control framework. The existence and necessary conditions for the minimization of the objective function were obtained, and numerical results were obtained by applying the projected gradient method and the two-parameter model function method to the minimization problem. Chorfi-El Guermai-Maniar-Zouhair [10] investigated a class of inverse hyperbolic problems for the wave equation with dynamic boundary conditions. The main objective was to determine some forcing terms from the final overdetermination of the displacement. First, they investigated the Fréchet differentiability of the Tikhonov functional and derived a gradient formula by solving the corresponding auxiliary problem, thereby proving the Lipschitz continuity of the gradient. Furthermore, they discussed the existence and uniqueness of the minimization problem. Finally, they implemented the numerical experiment of internal wave force reconstruction via conjugating the gradient algorithm. Cannon-DuChateau [11] investigated the inverse problem of the unknown source term S from boundary information in the inverse problem of the wave equation. They derived several properties related to the solution of this initial margin problem, and they used these properties to demonstrate the existence of the unknown source term. Furthermore, preliminary numerical experimental results were provided to demonstrate the feasibility of identifying the unknown source term numerically. The above studies were performed on single-point data, and there was no superposition effect. For the Tikhonov variational approach with the choice of regularization parameters and the generalized discrepancy principle, please refer to this classic work, as the basic regularization methods are contained there: [12].

With the in-depth study of ground microseismic signal monitoring technology, researchers have found that, although the DAS system has demonstrated excellent performance in data acquisition, the performance of data processing and the analysis process face many challenges. The data at each acquisition point on the DAS system, which are called DAS-type data, are, in actuality, the superposition of acoustic data from several nearby points. This can be considered to be a projection of a segment of amplitude data onto a single acquisition point, thus adding complexity to the data analysis. The complexity is mainly due to the interference and superposition of acoustic waves, signal attenuation, ambient noise, spatial resolution limitations, and the intricacy of the mathematical model of the wave equations coupled with the challenges in solving the inverse problem. At the same time, the problem of missing data is often encountered when investigating the source term inversion of the two-dimensional wave equation, which directly affects the accuracy and reliability of the inversion. Missing data can be caused by a variety of reasons, such as sensor failures and data transmission problems. Incomplete data can lead to an inadequate understanding of the wavefield information, which, in turn, affects the inversion and the estimation of the properties of the source terms. These difficulties not only increase the difficulty of the inversion algorithm, but they may also lead to misinterpretation of the nature of the fluctuating source terms [13].

In this paper, we construct a new integral operator $\tilde{K}$, which maps the interior source $f \in L^2(\Omega)$ to the DAS-type data $g \geq 0$ on the boundary. It is important to note that, for any $g \geq 0$, we cannot guarantee the existence and uniqueness of f such that $\tilde{K}f = g$. In other words, for general $g \geq 0$, the nonlinear operator $\tilde{K}$ is not necessarily reversible. In addition, we prove that $\tilde{K}$ is not injective on $L^2(\Omega)$ in general, thus implying that the solution of $\tilde{K}f = g$ on $L^2(\Omega)$ may not be unique. Coupled with the instability of the $\tilde{K}$ operator, it can be seen that solving $\tilde{K}f = g$ may not satisfy all three conditions of well posedness. Here,

one cannot employ the Fourier transform approach to solve the inverse problem directly, because the DAS-type data are of the superposition type over the boundary of the finite region. In order to overcome the above difficulties, we introduced a minimizing problem on a compact convex subset of $L^2(\Omega)$ [14] and combined it with Tikhonov regularization, which exists in the unique minimizer. The regularization parameter was chosen via the GCV method. Finally, the least squares algorithm was used to solve the source function for numerical method. When considering the presence of noise in a real situation, inverting the measured data by adding 1% and 5% random noise perturbation can also obtain the proper results. In the case of a single source, the shape and position of the source term can still be inverted with one side of the data missing. However, the inversion of the source term function was incomplete with two sides of the data missing, which could be regarded as the missing information.

This article is organized as follows: In Section 2, the explicit form and derivation of the $\tilde{K}$ operator are delivered, where the interior source $f \in L^2(\Omega)$ is mapped to the DAS-type date $g \geq 0$ at the boundary, and a series of properties of the operator $\tilde{K}$ that are related to the ill posedness of the inverse problem are investigated. In Section 3, we introduce a proper minimizing problem for the inverse problem, which is proven to be well posed. Lastly, the numerical examples for different cases are given in Section 4.

2. Wave Transmission and DAS-Type Data

2.1. Wave Transmission

The wave was assumed to occur in $\Omega = [0, L_1] \times [0, L_2]$, as shown in Figure 1. Without a loss of generality, we assumed the position of the wave source was at (x_0, y_0), as shown by the red center point in Figure 1. Unlike a single-point sensor, DAS collects the superposition of the absolute values of the amplitudes in a section of the cable. This is conducted, as taking the endpoints may lead to interference with the data from the neighboring edges (which is not desirable, as these endpoints are avoided in the data collection). As shown in Figure 1, Edge l_1 is $y = 0$, $x \in [dl, L_1 - dl]$; Edge l_2 is $x = L_1$, $y \in [dl, L_1 - dl]$; Edge l_3 is $y = L_2$, $x \in [dl, L_1 - dl]$; Edge l_4 is $x = 0$, $y \in [dl, L_2 - dl]$; and dl is the length of the superimposition. And, the data collection set was $S = l_1 \cup l_2 \cup l_3 \cup l_4$, which has been marked in red. Through denoting the amplitude at point (x, y) as $u(x, y)$, the data collected at point $(x, L_2) \in l_3$ are the superposition of the absolute value of the amplitudes in the interval $(x, x + dl)$, as shown by the green line segment on Edge l_3 in Figure 1, which is $\int_x^{x+dl} |u(x, L_2)| dx$. Similarly, the data collected at point $(L_1, y) \in l_2$ is the superposition of the absolute value of the amplitude within the interval $(y, y + dl)$, as shown by the green line segment on the edge l_2 in Figure 1, which is $\int_y^{y+dl} |u(L_1, y)| dy$.

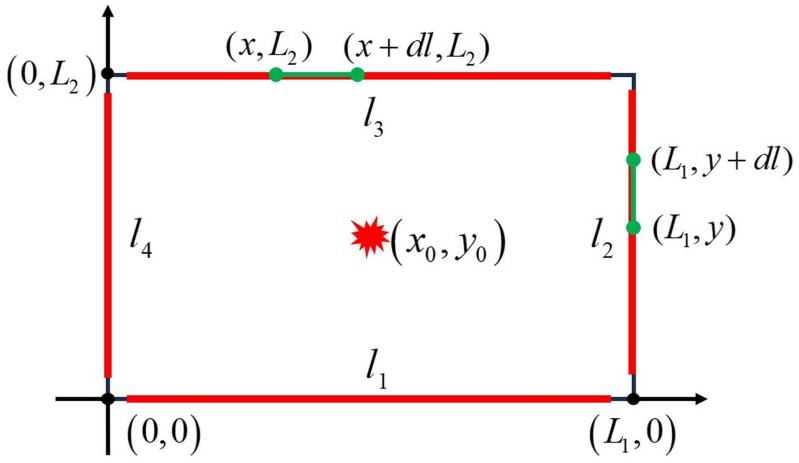

Figure 1. Wave propagation model.

The propagation model of the wave source satisfies the following wave equation:

$$\begin{aligned} \frac{\partial^2 u}{\partial t^2} &= c^2\left(\frac{\partial^2 u}{\partial x^2} + \frac{\partial^2 u}{\partial y^2}\right) + f(x,y,t), \quad (x,y) \in \mathbb{R}^2, t \geq 0, \\ u(x,y,0) &= \varphi(x,y), \quad u_t(x,y,0) = \psi(x,y), \quad (x,y) \in \mathbb{R}^2, \end{aligned} \tag{1}$$

where c is the wave speed, and $f \in C^2(\Omega \times [0,\infty))$ has its support inside Ω, $\varphi \in C^3(\Omega)$ and $\psi \in C^2(\Omega)$. The function $u(x,y,t)$ is the solution to the problem described above. According to the formula for the solution of the two-dimensional wave equation, we have the following [15]:

$$\begin{aligned} u(x,y,t) =& \frac{1}{2\pi c}\frac{\partial}{\partial t}\iint\limits_{B_{ct}(x,y)} \frac{\varphi(\tilde{x},\tilde{y})}{\sqrt{c^2(t-\tau)^2-(x-\tilde{x})^2-(y-\tilde{y})^2}} d\tilde{x}d\tilde{y} \\ &+ \frac{1}{2\pi c}\iint\limits_{B_{ct}(x,y)} \frac{\psi(\tilde{x},\tilde{y})}{\sqrt{c^2(t-\tau)^2-(x-\tilde{x})^2-(y-\tilde{y})^2}} d\tilde{x}d\tilde{y} \\ &+ \frac{1}{2\pi c}\int_0^t \iint\limits_{B_{c(t-\tau)}(x,y)} \frac{f(\tilde{x},\tilde{y},\tau)}{\sqrt{c^2(t-\tau)^2-(x-\tilde{x})^2-(y-\tilde{y})^2}} d\tilde{x}d\tilde{y}\, d\tau. \end{aligned} \tag{2}$$

Since the oscillations occurred instantaneously, we assumed that $\psi = \phi = 0$ and that f only occurs at time $t = 0$ in $\Omega = [0, L_1] \times [0, L_2]$. Then, based on (2), the solution was found to have the following form:

$$u(x,y,t) = \int_0^{L_2}\int_0^{L_1} f(\tilde{x},\tilde{y}) G(x,y,t;\tilde{x},\tilde{y},0)\, d\tilde{x}d\tilde{y}, \tag{3}$$

where

$$G(x,y,t;\tilde{x},\tilde{y},0) = \frac{1}{2\pi c}\frac{I_{(x-\tilde{x})^2+(y-\tilde{y})^2<c^2t^2}}{\sqrt{c^2t^2-(x-\tilde{x})^2-(y-\tilde{y})^2}}, \tag{4}$$

$$I_{(x-\tilde{x})^2+(y-\tilde{y})^2<c^2t^2} = \begin{cases} 1 & \text{if } (x-\tilde{x})^2+(y-\tilde{y})^2 < c^2t^2, \\ 0 & \text{if } (x-\tilde{x})^2+(y-\tilde{y})^2 \geq c^2t^2. \end{cases} \tag{5}$$

For $T > 0$,

$$(Kf)(x,y) = \int_0^{L_2}\int_0^{L_1} H(x,y;\tilde{x},\tilde{y}) f(\tilde{x},\tilde{y})\, d\tilde{x}d\tilde{y} = u(x,y,T), \tag{6}$$

where

$$H(x,y;\tilde{x},\tilde{y}) = G(x,y,T;\tilde{x},\tilde{y},0). \tag{7}$$

Via the compactness argument, the definition of Kf can be extended to $L^2(\Omega)$.

2.2. Operator Formula

Since the collected data were the accumulation of the absolute amplitudes measured on the boundary, the case of $f \geq 0$ was first considered below. Evidently, $H(x,y;\tilde{x},\tilde{y}) \geq 0$, and, for $f \geq 0$, there is $Kf \geq 0$, i.e., $u \geq 0$. Therefore, we define the function set here as follows:

$$L^2_+(\Omega) = \{f | f \in L^2(\Omega), f \geq 0\}. \tag{8}$$

It can be defined similarly as

$$L^2_-(\Omega) = \{f | f \in L^2(\Omega), f \leq 0\}, \tag{9}$$

and $L^2_\pm(\Omega) = L^2_+(\Omega) \cup L^2_-(\Omega)$. Similarly, we can define $L^2_+(S) = \{f | f \in L^2(S), f \geq 0\}$.

Next, we consider the $f \in L^2_+(\Omega)$ case first. Using Fubini's theorem, the measured value $g(x, y, T)$ at point $(x, y) \in l_3$ is

$$g(x, L_2, T) = \int_0^{L_2} \int_0^{L_1} \left(\int_x^{x_l} H(\hat{x}, L_2; \tilde{x}, \tilde{y})\, d\hat{x} \right) f(\tilde{x}, \tilde{y})\, d\tilde{x} d\tilde{y}, \tag{10}$$

with $x_l = x + dl$ (see Appendix A, (A1)). Thus, the kernel function $H(x, y; \tilde{x}, \tilde{y})$ was integrated in the x and y directions, respectively, to obtain the new kernel function $\hat{H}(x, y; \tilde{x}, \tilde{y})$. For the explicit expression of $\hat{H}(x, y; \tilde{x}, \tilde{y})$, we can construct the functions $\hat{H}_{l_1}(x, y; \tilde{x}, \tilde{y})$, $\hat{H}_{l_2}(x, y; \tilde{x}, \tilde{y})$, $\hat{H}_{l_3}(x, y; \tilde{x}, \tilde{y})$, and $\hat{H}_{l_4}(x, y; \tilde{x}, \tilde{y})$ (see Appendix A).

From Formulas (A9) and (A17), we were able to obtain the new kernel function

$$\hat{H}(x, y; \tilde{x}, \tilde{y}) = \begin{cases} \hat{H}_{l_1}(x, y; \tilde{x}, \tilde{y}), & (x, y) \in l_1, \\ \hat{H}_{l_2}(x, y; \tilde{x}, \tilde{y}), & (x, y) \in l_2, \\ \hat{H}_{l_3}(x, y; \tilde{x}, \tilde{y}), & (x, y) \in l_3, \\ \hat{H}_{l_4}(x, y; \tilde{x}, \tilde{y}), & (x, y) \in l_4, \end{cases} \tag{11}$$

and $\hat{H}(x, y; \tilde{x}, \tilde{y}) \geq 0$. Therefore, we constructed a new integral operator, which maps the source term $f(x, y) \in L^2_+(\Omega)$ to the DAS-type data $g(x, y) \in L^2_+(S)$ as follows:

$$g(x, y) = (\tilde{K}f)(x, y) = \int_0^{L_2} \int_0^{L_1} \hat{H}(x, y; \tilde{x}, \tilde{y}) f(\tilde{x}, \tilde{y})\, d\tilde{x} d\tilde{y}. \tag{12}$$

Then, for $f \in L^2_-(\Omega)$, $(\tilde{K}f)(x, y)$ can be defined as

$$(\tilde{K}f)(x, y) = -\int_0^{L_2} \int_0^{L_1} \hat{H}(x, y; \tilde{x}, \tilde{y}) f(\tilde{x}, \tilde{y})\, d\tilde{x} d\tilde{y} \geq 0. \tag{13}$$

For $f \in L^2(\Omega)$, we defined $f_+ = \max\{f, 0\}$, $f_- = \min\{f, 0\}$, where $f_+ \in L^2_+(\Omega)$, and $f_- \in L^2_-(\Omega)$, with $f = f_+ + f_-$. Due to the superposition of the absolute value of the DAS-type amplitude, we obtained

$$\begin{aligned} (\tilde{K}f)(x, y) &= \left| \int_0^{L_2} \int_0^{L_1} \hat{H}(x, y; \tilde{x}, \tilde{y}) f_+(\tilde{x}, \tilde{y})\, d\tilde{x} d\tilde{y} + \int_0^{L_2} \int_0^{L_1} \hat{H}(x, y; \tilde{x}, \tilde{y}) f_-(\tilde{x}, \tilde{y})\, d\tilde{x} d\tilde{y} \right| \\ &= \left| \int_0^{L_2} \int_0^{L_1} \hat{H}(x, y; \tilde{x}, \tilde{y}) f(\tilde{x}, \tilde{y})\, d\tilde{x} d\tilde{y} \right|. \end{aligned} \tag{14}$$

2.3. Properties of the Operator

As the direct consequence of $\tilde{K}f$, we obtained the following two properties.

Property 1. *The operator $\tilde{K}$ is not a linear operator on $L^2(\Omega)$.*

Unlike the inverse problem with single-point data, DAS-type data lead to a noninjective property.

Property 2. *For $L^2(\Omega) \setminus L^2_{\pm}(\Omega)$, the operator $\tilde{K}$ is not injective.*

Proof. Taking $f \in L^2(\Omega)$ with $f \neq -f$ implies $f \notin L^2_{\pm}(\Omega)$. Then,

$$g_1(x, y) = \tilde{K}f = \left| \int_0^{L_2} \int_0^{L_1} \hat{H}(x, y; \tilde{x}, \tilde{y}) f(\tilde{x}, \tilde{y})\, d\tilde{x} d\tilde{y} \right|, \tag{15}$$

$$\begin{aligned} g_2(x,y) = \tilde{K}(-f) =& \left| \int_0^{L_2} \int_0^{L_1} \hat{H}(x,y;\tilde{x},\tilde{y})(-f)(\tilde{x},\tilde{y})\, d\tilde{x}d\tilde{y} \right| \\ =& \left| \int_0^{L_2} \int_0^{L_1} \hat{H}(x,y;\tilde{x},\tilde{y}) f(\tilde{x},\tilde{y})\, d\tilde{x}d\tilde{y} \right| \\ =& g_1(x,y). \end{aligned} \tag{16}$$

As such, the operator $\tilde{K}$ is not injective. □

The mapping from single point sense data $u(x,y)$ to DAS-type data $g(x,y)$ is also not injective. Next, we took Edge l_3, which can extend to S easily, as an example. The definition of absolute values in DAS-type data, denoted as $g(x,L_2) = \int_x^{x+dl} |u(\hat{x},L_2)| d\hat{x}$, allowed us to construct examples similar to the above. Furthermore, it would show them as injective even for the $u(\hat{x},L_2) \geq 0$ case. When taking the positive function $v(x)$ with period dl, without a loss of generality, we assumed $\frac{1}{dl}\int_0^{dl} v(x)dx = 1$. Then, for any integer $k > 0$, we obtained

$$\int_x^{x+dl} v(k\hat{x})d\hat{x} = k\int_0^{\frac{dl}{k}} v(k\hat{x})d\hat{x} = \int_0^{\frac{dl}{k}} v(k\hat{x})dk\hat{x} = \int_0^{dl} v(s)ds \equiv dl. \tag{17}$$

Then, $v(kx)$ for $x \in \mathbb{N}$ and 1 corresponded to the same DAS-type data $g(x,y) \equiv dl$, which indicates the noninjectivity.

Property 3. *The operator $\tilde{K}$ is a bounded operator on $L^2(\Omega)$.*

Proof. For a given $(\tilde{x},\tilde{y}) \in \Omega$ for any $(x,y) \in S$, via (A9) and (A17), we can obtain

$$0 \leq \hat{H}^2(x,y;\tilde{x},\tilde{y}) \leq \left(\frac{1}{2\pi c}\right)^2 \pi^2 \leq \frac{1}{4c^2}. \tag{18}$$

Therefore, we can obtain

$$\begin{aligned} \left\|(\tilde{K}f)(x,y)\right\|_{L^2(S)} =& \left\| \int_0^{L_2} \int_0^{L_1} \hat{H}(x,y;\tilde{x},\tilde{y}) f(\tilde{x},\tilde{y})\, d\tilde{x}d\tilde{y} \right\|_{L^2(S)} \\ \leq& \left\| \frac{\sqrt{L_1L_2}}{4c^2} \|f\|_{L^2(\Omega)} \right\|_{L^2(S)} \\ \leq& \frac{\sqrt{2(L_1+L_2-4dl)L_1L_2}}{4c^2} \|f\|_{L^2(\Omega)}. \end{aligned} \tag{19}$$

As such, $\tilde{K}$ is a bounded operator from $L^2(\Omega)$ to $L^2_+(S)$. □

Next, we discuss the instability of the integral operator $\tilde{K}$. We defined the noise as $\delta_\omega = \beta_\omega \sin(\omega x)\sin(\omega y)$ and the measured data as $\hat{f}(x,y) = f(x,y) + \delta_\omega$. It was assumed below that $f \geq c > 0$ on Ω. The general conclusion can be obtained by changing the support set of the noise. We selected β_ω such that $\hat{f} \in L^2_+(\Omega)$; thus, we obtained

$$\begin{aligned}\left\|\hat{f}-f\right\|_{L^2(\Omega)}^2 &= \int_0^{L_2}\int_0^{L_1}\beta_\omega^2\sin^2(\omega x)\sin^2(\omega y)\,dxdy\\ &= \frac{\beta_\omega^2}{4}\int_0^{L_2}\int_0^{L_1}[1-\cos(2\omega x)][1-\cos(2\omega y)]\,dxdy\\ &= \frac{\beta_\omega^2}{4}\int_0^{L_2}\int_0^{L_1}[1-\cos(2\omega x)-\cos(2\omega y)+\cos(2\omega x)\cos(2\omega y)]\,dxdy\\ &= \frac{\beta_\omega^2}{4}\int_0^{L_2}\left[L_1-\frac{1}{2\omega}\sin(2\omega L_1)-L_1\cos(2\omega y)+\frac{1}{2\omega}\sin(2\omega L_1)\cos(2\omega y)\right]dy\\ &= \frac{\beta_\omega^2}{4}\left[L_1L_2-\frac{L_2}{2\omega}\sin(2\omega L_1)-\frac{L_1L_2}{2\omega}\sin(2\omega L_2)+\frac{1}{4\omega^2}\sin(2\omega L_1)\cos(2\omega L_2)\right].\end{aligned} \tag{20}$$

For l_3, we have

$$\begin{aligned}\left\|\tilde{K}\hat{f}-\tilde{K}f\right\|_{L^2(l_3)}^2 =& \left\|\tilde{K}(\hat{f}-f)\right\|_{L^2(l_3)}^2\\ =& \beta_\omega^2\frac{1}{2\omega^2}\sin^2\sqrt{2}T\sin^2\omega L_2\int_{dl}^{L_1-dl}\left(\int_x^{x+dl}\sin\omega\hat{x}d\hat{x}\right)^2dx\\ \leq& \beta_\omega^2\frac{1}{2\omega^2}\sin^2\sqrt{2}T\sin^2\omega L_2 dl^2(L_1-dl).\end{aligned} \tag{21}$$

It is easy to see that as $\omega\to\infty$, the error in the data is $\left\|\tilde{K}\hat{f}-\tilde{K}f\right\|_{L^2(S)}^2\to 0$, while the error in the solution is $\left\|\hat{f}-f\right\|_{L^2(\Omega)}^2\to\frac{\beta_\omega^2}{4}L_1L_2>0$ [16]. As such, the DAS-type data $g(x,y)$ do not continuously depend on the source $f(x,y)$, which implies the following property.

Property 4. *The operator $\tilde{K}$ is not stable.*

3. Formulation of the Inverse Problem

In this section, we would like to consider the proper inverse problem of $\tilde{K}f=g$. Via (14), the DAS-type data g are the absolute value of the convolution of the source term f and the non-negative kernel $\hat{H}$, which indicates that $\tilde{K}$ is from $L^2(\Omega)$ to $L^2_+(S)$. A typical path of solving $\tilde{K}f=g$ is to find the minimizer of $\left\|\tilde{K}f-g\right\|_{L^2(S)}^2$. However, Property 2 shows that the solutions of $\tilde{K}f=g$ in $L^2(\Omega)$ are not unique, which also implies the that minimizing problem $\left\|\tilde{K}f-g\right\|_{L^2(S)}^2$ does not have the unique minimizer in $L^2(\Omega)$. For the uniqueness, we considered the minimizing problem on $L^2_+(\Omega)$. Additionally, Property 4 indicates the possible instability of the inversion of $\tilde{K}f=g$. As such, we introduced the minimization functional $J_\alpha(f)$ with Tikhonov regularization as follows:

$$J_\alpha(f)=\left\|\tilde{K}f-g\right\|_{L^2(S)}^2+\alpha\|f\|_{L^2(\Omega)}^2, \tag{22}$$

where $\alpha\|f\|_{L^2(\Omega)}^2$ is the Tikhonov regularization. Then, we obtained the following property:

Property 5. *Minimizing problem $\min_{f\in L^2_+(\Omega)}J_\alpha(f)$ exists as a unique minimizer.*

Proof. Via (22), we have

$$\alpha\|f\|_{L^2(\Omega)}^2\leq J_\alpha(f)\leq\left\|\tilde{K}f\right\|_{L^2(S)}^2+\|g\|_{L^2(S)}^2+\alpha\|f\|_{L^2(\Omega)}^2\leq\beta\|f\|_{L^2(\Omega)}^2+\|g\|_{L^2(S)}^2, \tag{23}$$

which shows the coercivity of the operator. For the existence part, $\min_{f\in L^2(\Omega)} I_\alpha(f)$, while

$$I_\alpha(f) = \left\|\tilde{H} * |f| - g\right\|^2_{L^2(S)} + \alpha\|f\|^2_{L^2(\Omega)}, \tag{24}$$

which is equal to the original problem $\min_{f\in L^2_+(\Omega)} J_\alpha(f)$. With Coercivity (23), the lower semicontinuity of $\|\cdot\|_{L^2(S)}$ and $\|\cdot\|_{L^2(\Omega)}$, $I_\alpha(f)$ has at least one minimizer in $L^2(\Omega)$, which implies that $J_\alpha(f)$ has at least one minimizer in $L^2_+(\Omega)$. Since $\tilde{K}f$ is linear with respect to $f \in L^2_+(\Omega)$, the strict convexity of norm $\|\cdot\|_{L^2(S)}$ and $\|\cdot\|_{L^2(\Omega)}$ naturally leads to the strict convexity of $J_\alpha(f)$, which implies that the minimizer is unique. □

Via the above property, we can conclude that there exists a unique reachable elements of $\min_{f\in L^2_{+,d}(\Omega)} J_\alpha(f)$.

4. Numerical Examples

Through the above derivation, we can obtain the operator form of the inverse problem as follows:

$$\tilde{K}f(x,y) = \int_0^{L_2}\int_0^{L_1} \hat{H}(x,y;\tilde{x},\tilde{y}) f(\tilde{x},\tilde{y})\, d\tilde{x}d\tilde{y} = g(x,y). \tag{25}$$

According to the definition of the integral and the calculation formula of the numerical integral, we have

$$g(x_p,y_q) = \sum_{j=1}^{N_y}\sum_{i=1}^{N_x} \hat{H}(x_p,y_q;\tilde{x}_i,\tilde{y}_j) f(\tilde{x}_i,\tilde{y}_j)\Delta\tilde{x}_i\Delta\tilde{y}_j. \tag{26}$$

We meshed Ω, where the x direction was divided into $N_x - 1$ parts, and the y direction was divided into $N_y - 1$ parts, where x_p, x_i, y_q, y_j are the x direction nodes and y direction nodes for $p = 1,2,\ldots,N_x$, $q = 1,2,\ldots,N_y$, $i = 1,2,\ldots,N_x$, and $j = 1,2,\ldots,N_y$, and $\Delta x = \frac{L_1}{N_x-1}, \Delta y = \frac{L_2}{N_y-1}, dl = d_L\Delta x$. In subsequent numerical experiments, d_L was set to 5 and $\Delta x = \Delta y$.

According to the above derivation, in order to ensure that the total number of meshing nodes was equal to the total number of measurement data, the number of measurement data points on each edge was set to $N_L = \lfloor N_xN_y/4 \rfloor + d_L$ for the source term inversion of the superimposed data on the regional boundary S.

Here, $(\tilde{x}_i,\tilde{y}_j)$ is the meshing node. For the measured data, the value was taken at the (x_p,y_q) point. When $(x_p,y_q) \in S$, take $x_1 = y_1 = dl$, and let $\hat{H}^{p,q}_{i,j} = \hat{H}(x_p,y_q;\tilde{x}_i,\tilde{y}_j)\Delta\tilde{x}_i\Delta\tilde{y}_j$, $g(x_p,y_q)$ be the actual measurement data, which are obtained by the finite difference method as a numerical solution to the wave equation and accumulation of data as measurement data. This constructs the data with the same characteristics as the data collected by DAS using the following equation:

(1) When $(x_p,y_q) \in l_1$, there is the equation $\hat{H}^{l_1}\hat{f} = g^{l_1}$, where

$$\hat{H}^{l_1} = \begin{bmatrix} \hat{H}^{1,1}_{1,1} & \hat{H}^{1,1}_{1,2} & \cdots & \hat{H}^{1,1}_{1,N_y} & \cdots & \hat{H}^{1,1}_{N_x,1} & \cdots & \hat{H}^{1,1}_{N_x,N_y} \\ \hat{H}^{2,1}_{1,1} & \hat{H}^{2,1}_{1,2} & \cdots & \hat{H}^{2,1}_{1,N_y} & \cdots & \hat{H}^{2,1}_{N_x,1} & \cdots & \hat{H}^{2,1}_{N_x,N_y} \\ \vdots & \vdots & \ddots & \vdots & \ddots & \vdots & \ddots & \vdots \\ \hat{H}^{N_L-d_L,1}_{1,1} & \hat{H}^{N_L-d_L,1}_{1,2} & \cdots & \hat{H}^{N_L-d_L,1}_{1,N_y} & \cdots & \hat{H}^{N_L-d_L,1}_{N_x,1} & \cdots & \hat{H}^{N_L-d_L,1}_{N_x,N_y} \end{bmatrix}, \tag{27}$$

$$g^{l_1} = \begin{bmatrix} g(x_1,y_1) \\ g(x_2,y_1) \\ \vdots \\ g(x_{N_L-d_L},y_1) \end{bmatrix}. \tag{28}$$

(2) When $(x_p, y_q) \in l_2$, there is the equation $\hat{H}^{l_2}\hat{f} = g^{l_2}$, where

$$\hat{H}^{l_2} = \begin{bmatrix} \hat{H}_{1,1}^{N_x,1} & \hat{H}_{1,2}^{N_x,1} & \cdots & \hat{H}_{1,N_y}^{N_x,1} & \cdots & \hat{H}_{N_x,1}^{N_x,1} & \cdots & \hat{H}_{N_x,N_y}^{N_x,1} \\ \hat{H}_{1,1}^{N_x,2} & \hat{H}_{1,2}^{N_x,2} & \cdots & \hat{H}_{1,N_y}^{N_x,2} & \cdots & \hat{H}_{N_x,1}^{N_x,2} & \cdots & \hat{H}_{N_x,N_y}^{N_x,2} \\ \vdots & \vdots & \ddots & \vdots & \ddots & \vdots & \ddots & \vdots \\ \hat{H}_{1,1}^{N_x,N_L-d_L} & \hat{H}_{1,2}^{N_x,N_L-d_L} & \cdots & \hat{H}_{1,N_y}^{N_x,N_L-d_L} & \cdots & \hat{H}_{N_x,1}^{N_x,N_L-d_L} & \cdots & \hat{H}_{N_x,N_y}^{N_x,N_L-d_L} \end{bmatrix}, \tag{29}$$

$$g^{l_2} = \begin{bmatrix} g(x_{N_x}, y_1) \\ g(x_{N_x}, y_2) \\ \vdots \\ g(x_{N_x}, y_{N_L-d_L}) \end{bmatrix}. \tag{30}$$

(3) When $(x_p, y_q) \in l_3$, there is the equation $\hat{H}^{l_3}\hat{f} = g^{l_3}$, where

$$\hat{H}^{l_3} = \begin{bmatrix} \hat{H}_{1,1}^{1,N_y} & \hat{H}_{1,2}^{1,N_y} & \cdots & \hat{H}_{1,N_y}^{1,N_y} & \cdots & \hat{H}_{N_x,1}^{1,N_y} & \cdots & \hat{H}_{N_x,N_y}^{1,N_y} \\ \hat{H}_{1,1}^{2,N_y} & \hat{H}_{1,2}^{2,N_y} & \cdots & \hat{H}_{1,N_y}^{2,N_y} & \cdots & \hat{H}_{N_x,1}^{2,N_y} & \cdots & \hat{H}_{N_x,N_y}^{2,N_y} \\ \vdots & \vdots & \ddots & \vdots & \ddots & \vdots & \ddots & \vdots \\ \hat{H}_{1,1}^{N_L-d_L,N_y} & \hat{H}_{1,2}^{N_L-d_L,N_y} & \cdots & \hat{H}_{1,N_y}^{N_L-d_L,N_y} & \cdots & \hat{H}_{N_x,1}^{N_L-d_L,N_y} & \cdots & \hat{H}_{N_x,N_y}^{N_L-d_L,N_y} \end{bmatrix}, \tag{31}$$

$$g^{l_3} = \begin{bmatrix} g(x_1, y_{N_y}) \\ g(x_2, y_{N_y}) \\ \vdots \\ g(x_{N_L-d_L}, y_{N_y}) \end{bmatrix}. \tag{32}$$

(4) When $(x_p, y_q) \in l_4$, there is the equation $\hat{H}^{l_4}\hat{f} = g^{l_4}$, where

$$\hat{H}^{l_4} = \begin{bmatrix} \hat{H}_{1,1}^{1,1} & \hat{H}_{1,2}^{1,1} & \cdots & \hat{H}_{1,N_y}^{1,1} & \cdots & \hat{H}_{N_x,1}^{1,1} & \cdots & \hat{H}_{N_x,N_y}^{1,1} \\ \hat{H}_{1,1}^{1,2} & \hat{H}_{1,2}^{1,2} & \cdots & \hat{H}_{1,N_y}^{1,2} & \cdots & \hat{H}_{N_x,1}^{1,2} & \cdots & \hat{H}_{N_x,N_y}^{1,2} \\ \vdots & \vdots & \ddots & \vdots & \ddots & \vdots & \ddots & \vdots \\ \hat{H}_{1,1}^{1,N_L-d_L} & \hat{H}_{1,2}^{1,N_L-d_L} & \cdots & \hat{H}_{1,N_y}^{1,N_L-d_L} & \cdots & \hat{H}_{N_x,1}^{1,N_L-d_L} & \cdots & \hat{H}_{N_x,N_y}^{1,N_L-d_L} \end{bmatrix}, \tag{33}$$

$$g^{l_4} = \begin{bmatrix} g(x_1, y_1) \\ g(x_1, y_2) \\ \vdots \\ g(x_1, y_{N_L-d_L}) \end{bmatrix}. \tag{34}$$

From the (27)–(34) formula, we can see that the equation of the inversion source term $f(x, y)$ is as follows:

$$\begin{bmatrix} \hat{H}^{l_1} \\ \hat{H}^{l_2} \\ \hat{H}^{l_3} \\ \hat{H}^{l_4} \end{bmatrix} \hat{f} = \begin{bmatrix} g^{l_1} \\ g^{l_2} \\ g^{l_3} \\ g^{l_4} \end{bmatrix}, \tag{35}$$

where

$$\hat{f} = \left[f(\tilde{x}_1, \tilde{y}_1), f(\tilde{x}_1, \tilde{y}_2), \cdots, f(\tilde{x}_1, \tilde{y}_{N_y}), \cdots, f(\tilde{x}_{N_x}, \tilde{y}_1), \cdots, f(\tilde{x}_{N_x}, \tilde{y}_{N_y}) \right]^T. \tag{36}$$

This paper used the source term functions of a single source and multiple sources to conduct numerical experiments. We conducted experiments under different levels of noise, as well as established and solved Equation (35).

We defined the numerical result error, and the L^2 error was

$$\begin{aligned} e &= \left\| f(x,y) - \hat{f}(x,y) \right\|_{L^2(\Omega)} \\ &= \left(\sum_{i=1}^{N_x} \sum_{j=1}^{N_y} \Delta x \Delta y \left(f(x_i,y_j) - \hat{f}(x_i,y_j) \right)^2 \right)^{\frac{1}{2}}, \end{aligned} \tag{37}$$

where $f(x_i, y_j)$ represents the function value of the source item at grid node (x_i, y_j), and $N_x N_y$ is the total number of grid nodes.

We defined the noise disturbance as follows:

$$g^\delta = g + \delta r \cdot g, \tag{38}$$

where $0 < \delta < 1$, $r = [r_k]_{N_x N_y \times 1} (0 < r_k < 1)$ is a random $N_x N_y$-dimensional column vector satisfying a continuous uniform distribution, and $r \cdot g = [r_k g_k]_{N_x N_y \times 1}$.

Then, we used the GCV generalized crossvalidation method [17] to select the regularization parameter α. GCV refers to a better method of calculating regularization parameters under the premise that the error estimate δ cannot be predicted. Here, we provide the definition of the GCV function for the parameter α as follows:

$$GCV(\alpha) = \frac{\left\| (I - \tilde{K} R_\alpha) g^\delta \right\|^2}{(tr(I - \tilde{K} R_\alpha))^2}, \tag{39}$$

where R_α is the regularization operator of operator $\tilde{K}$, $R_\alpha = (\alpha I + \tilde{K}^* \tilde{K})^{-1} \tilde{K}^*$. $\tilde{K}^*$ denotes the adjoint operator of the operator $\tilde{K}$, and tr denotes the sum of the diagonal elements of the square matrix (i.e., the trace of the matrix). The regularization parameter α is obtained when the GCV function reaches the minimum.

Numerical Example 1. *Let* $\varphi(x,y) = \psi(x,y) = 0$; *then, set* $L_1 = 4$, $L_2 = 4$, $N_x = 40$, $N_y = 40$, *wave speed* $c = 0.1$, $T = 20$, *and the source term function* $f(x,y) = c^2 e^{-c_1 r_0} \cdot \left[2c_1 c_2 (x^2 + y^2) - c_1^2 \right]$, *where* $(x_0, y_0) = (L_1/2, L_2/2)$, $c_1 = 4$, $c_2 = 10$, *and* $r_0 = (x - x_0)^2 + (y - y_0)^2$.

Figure 2a shows the graph of the source term function when the parameters were determined. Figures 3a, 4a and 5a display the numerical inversion results of the source term for the noise-free data, as well as the numerical inversion results of the source term with the addition of 1% and 5% noisy data, respectively. Different perturbations are listed in Table 1, along with the L^2 error result under the data condition and the regularization parameter selection result. As the noise level increased, the accuracy of the inversion results gradually decreased. In the absence of noise, the inversion results of the source term were particularly accurate, and the peak positions and shapes were consistent with expectations. After adding 1% noise, although the results were still good, subtle noise effects began to appear: the peak position slightly shifted, and there were some disturbances at the edges of the image. When the noise increased to 5%, the impact of the noise became more obvious: the accuracy of the inversion results decreased, the peak position and shape changed significantly, and the outline of the two-dimensional top view became blurred. As the noise level became larger, the regularization parameter also gradually became larger.

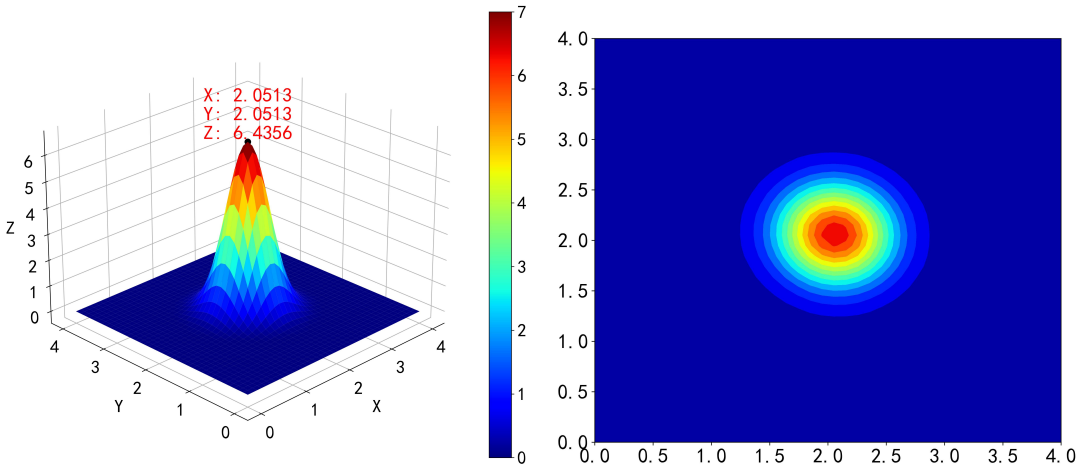

(**a**) (**b**)

Figure 2. The function graph of the source term $f(x,y) = c^2 e^{-c_1 r_0} \cdot \left[2c_1c_2(x^2+y^2) - c_1^2\right]$. (**a**) The source term function graph and (**b**) the top view of the source term function.

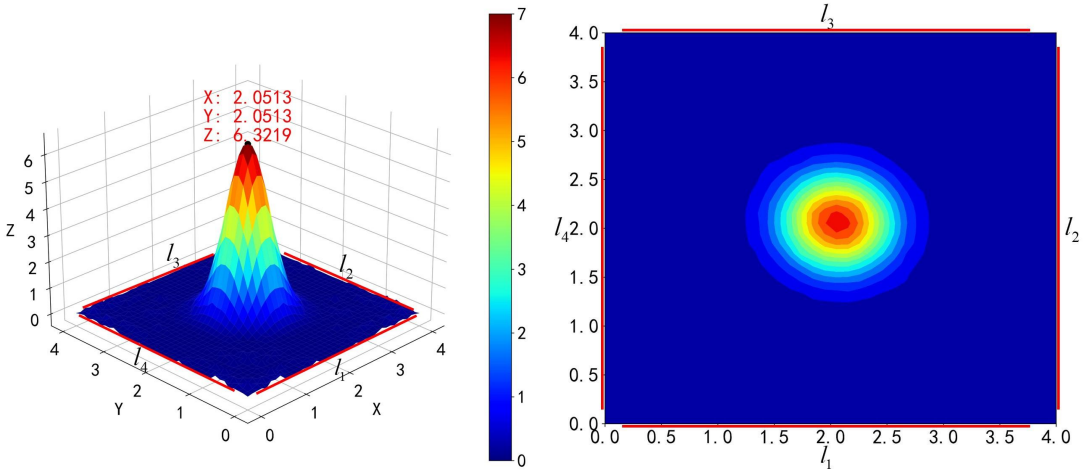

(**a**) (**b**)

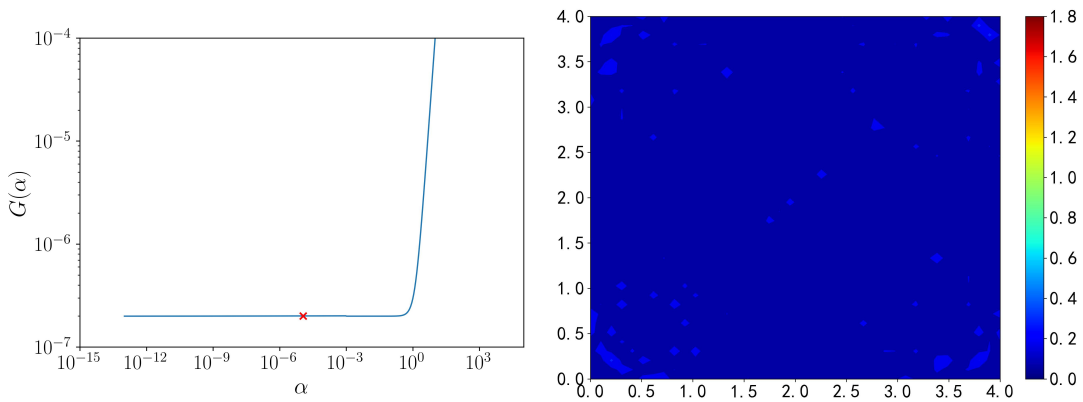

(**c**) (**d**)

Figure 3. The numerical inversion result of the source term $f(x,y) = c^2 e^{-c_1 r_0} \cdot \left[2c_1c_2(x^2+y^2) - c_1^2\right]$. (**a**) The numerical inversion result of the source term; (**b**) the top view of the inversion results; (**c**) the regularization parameter selection, red × indicates the selected regularization parameter; and the (**d**) the absolute value residual.

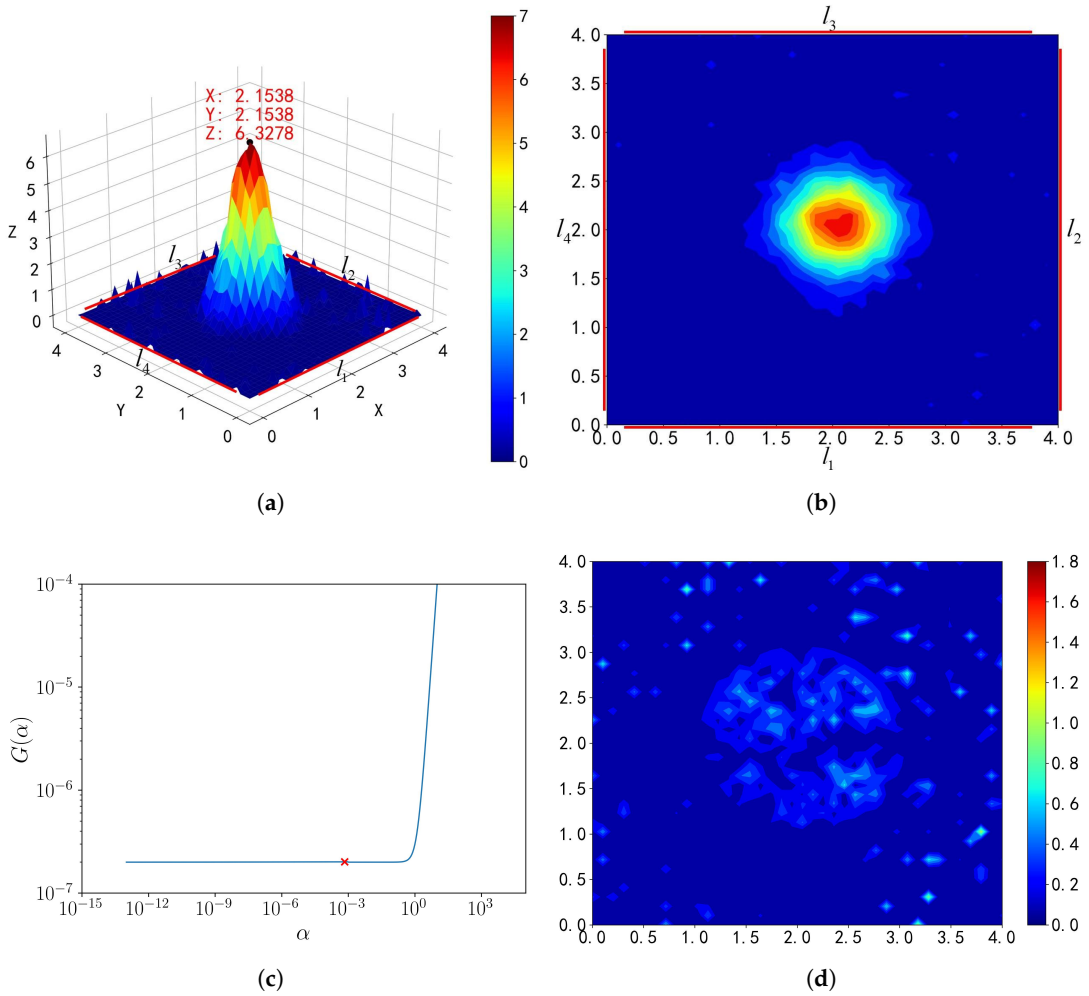

(**a**) (**b**)

(**c**) (**d**)

Figure 4. When $\delta = 1\%$, this shows the numerical inversion result of the source term $f(x,y) = c^2 e^{-c_1 r_0} \cdot \left[2c_1c_2(x^2+y^2) - c_1^2\right]$. (**a**) The numerical inversion result of the source term; (**b**) the top view of the inversion results; (**c**) the regularization parameter selection, red × indicates the selected regularization parameter; and (**d**) the absolute value residual.

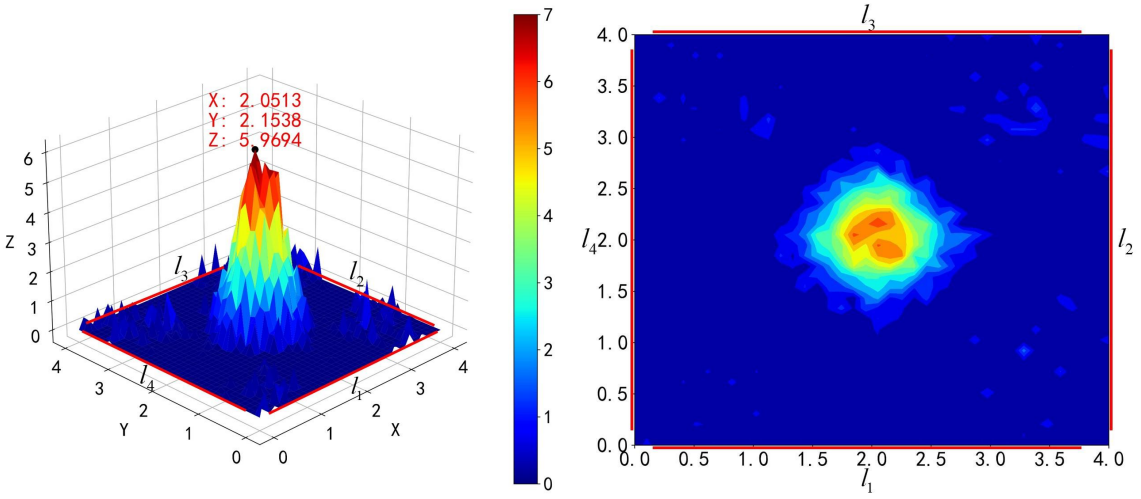

(**a**) (**b**)

Figure 5. *Cont.*

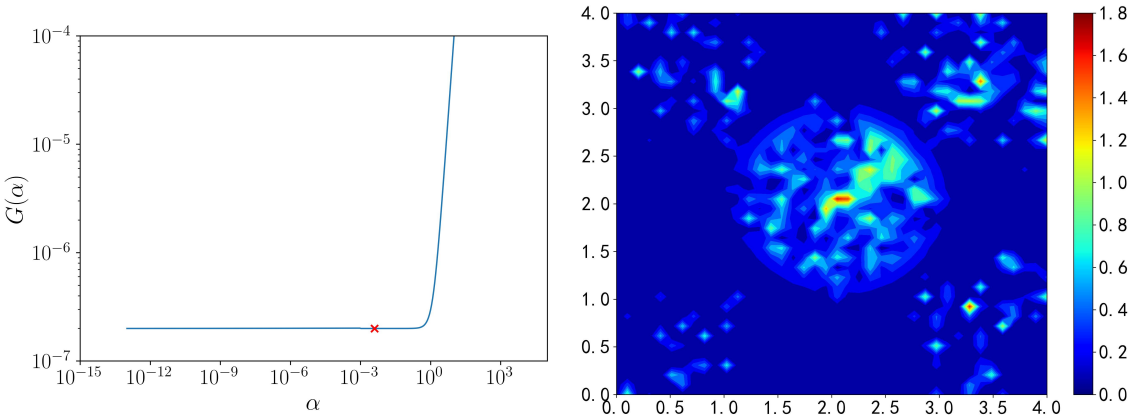

(**c**) (**d**)

Figure 5. When $\delta = 5\%$, this shows the numerical inversion result of the source term $f(x,y) = c^2 e^{-c_1 r_0} \cdot [2c_1c_2(x^2+y^2) - c_1^2]$. (**a**) The numerical inversion result of the source term; (**b**) the top view of the inversion results; (**c**) the regularization parameter selection, red × indicates the selected regularization parameter; and (**d**) the absolute value residual.

Table 1. The correlation coefficient changes with δ in single-source cases.

δ	e	α
0%	0.2336088	0.0000113
1%	0.6212708	0.0006808
5%	1.0499613	0.0039781

Figure 6a shows the inversion results in the absence of l_2 edge data. Despite the incomplete data, the inversion result still showed the basic shape of the source term function, which thus demonstrated that the inversion method can still provide some valid information, even with limited data. Figure 6b is a top view of the inversion results, which more clearly shows the distribution and concentration of the values in the inversion results. Figure 7a includes the inversion results that were obtained in the absence of l_1 and l_4 edge data, and the results show that the shape of the inversion performance deviated more from that of the source term function in the absence of additional data. From Figure 7b it can be seen that the inversion results demonstrated an obvious deviation from the shape of the source term function, thus indicating that more missing data on more edges will seriously affect the accuracy of the inversion results. Table 2 lists the L^2 error results that were obtained from inverting the source term when using data from different sides.

Table 2. The correlation coefficient changes obtained when using different edges.

Edge Used	e	α
l_1, l_2, l_3, l_4	0.2336088	0.0000113
l_1, l_2, l_3	0.8188965	0.0189262
l_2, l_3	1.9141931	0.1465854

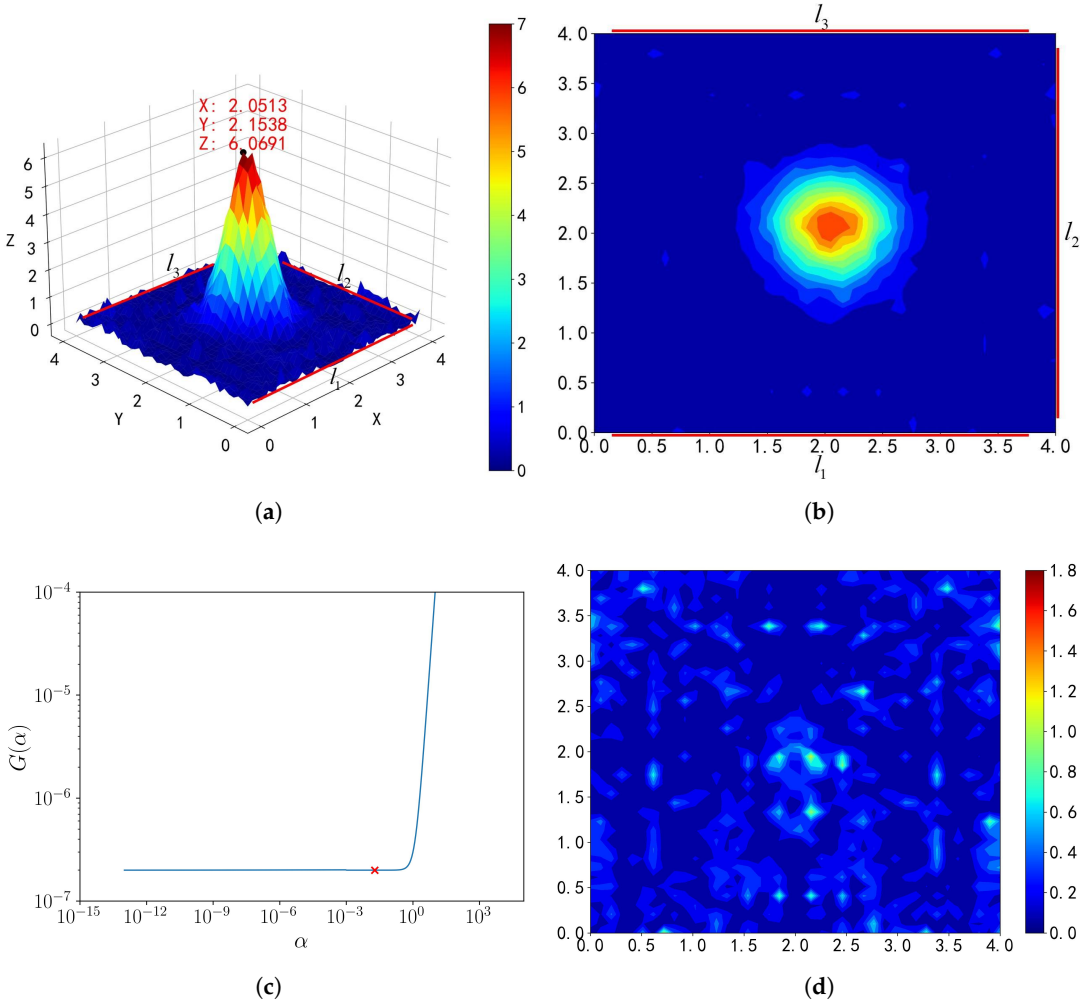

Figure 6. When the data of Edge l_2 were missing, the numerical inversion result of the source term was $f(x,y) = c^2 e^{-c_1 r_0} \cdot \left[2c_1 c_2 (x^2 + y^2) - c_1^2\right]$. (**a**) The numerical inversion result of the source term; (**b**) the top view of the inversion results; (**c**) the regularization parameter selection, red × indicates the selected regularization parameter; and (**d**) the absolute value residual.

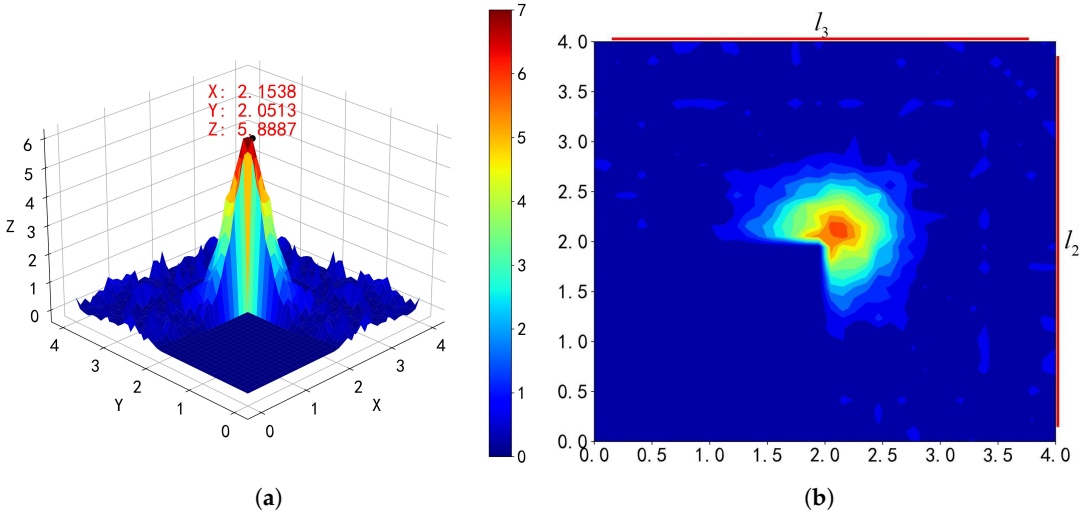

Figure 7. *Cont.*

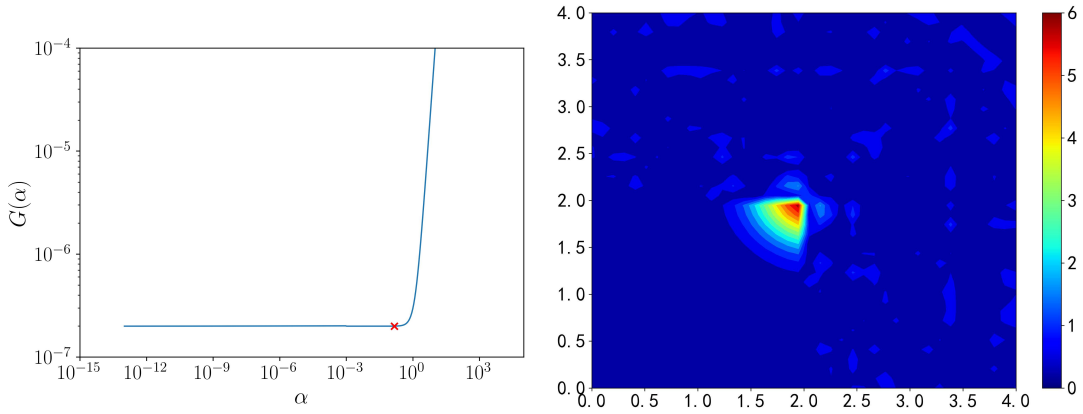

(**c**) (**d**)

Figure 7. When the data of Edges l_1 and l_4 were missing, the numerical inversion result of the source term was $f(x,y) = c^2 e^{-c_1 r_0} \cdot \left[2c_1c_2(x^2+y^2) - c_1^2\right]$. (**a**) The numerical inversion result of the source term; (**b**) the top view of the inversion results; (**c**) the regularization parameter selection, red × indicates the selected regularization parameter; and (**d**) the absolute value residual.

Numerical Example 2. *For the nonexponential source term function, we used values of* $L_1 = 4$, $L_2 = 4$, $N_x = 40$, $N_y = 40$, *wave speed* $c = 0.1$, $T = 20$, *and the source term function* $f(x,y) = \max\{0, 1 - \sqrt{r_0}\}$, *where* $(x_0, y_0) = (L_1/2, L_2/2)$, *and* $r_0 = (x - x_0)^2 + (y - y_0)^2$.

Figure 8a includes the source term function graph when the parameters were determined. Figures 9a, 10a, and 11a show the numerical inversion results of the source term for the noise-free data, as well as the numerical inversion results of the source term with the addition of 1% and 5% noisy data, respectively. The different perturbations are listed in Table 3 along with the L^2 error results under the data condition and regularization parameter selection results. This is different from the exponential form of the source term. The position, shape, and peak accuracy of the inversion result source term were found to go lower. This may be related to the smoothness of the bottom of the source term function. The inversion results with added noise also gradually decreased in accuracy, and the regularization parameters gradually became larger, like Numerical Example 1.

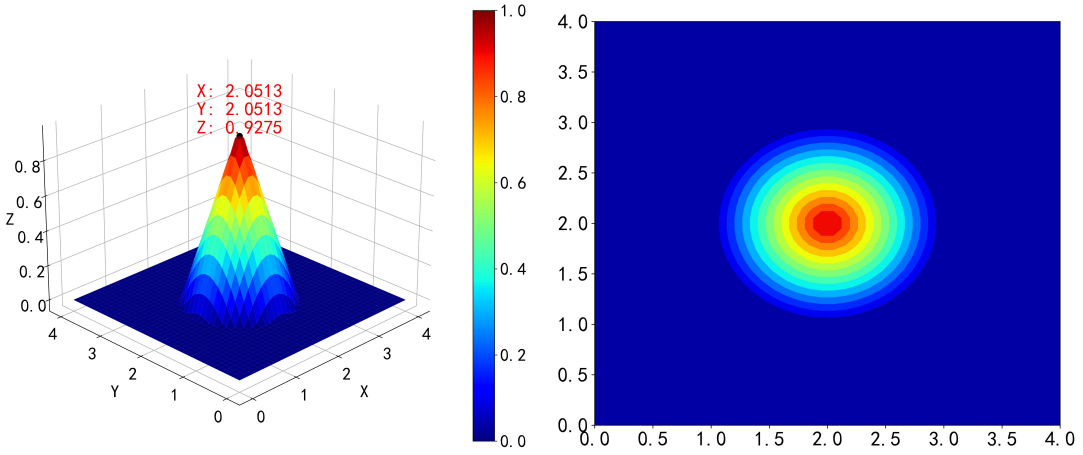

(**a**) (**b**)

Figure 8. A function graph of the source term $f(x,y) = c^2\left[e^{-c_1 r_0} + e^{-c_1 r_1}\right] \cdot \left[2c_1c_2(x^2+y^2) - c_1^2\right]$. (**a**) The source term function graph and (**b**) the top view of the source term function.

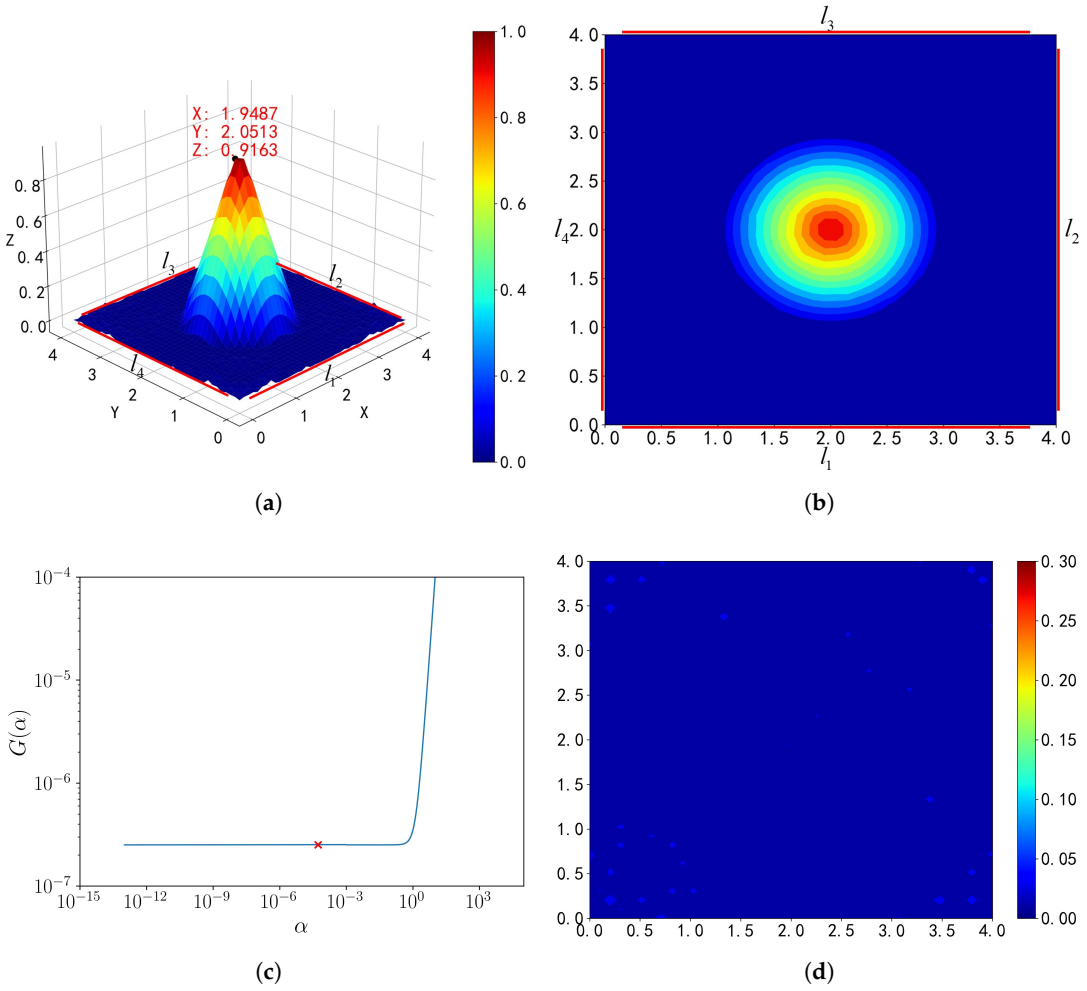

Figure 9. The numerical inversion result of the source term $f(x,y) = c^2\left[e^{-c_1 r_0} + e^{-c_1 r_1}\right] \cdot \left[2c_1c_2(x^2+y^2) - c_1^2\right]$. (**a**) The numerical inversion result of the source term; (**b**) the top view of the inversion results; (**c**) the regularization parameter selection, red × indicates the selected regularization parameter; and (**d**) the absolute value residual.

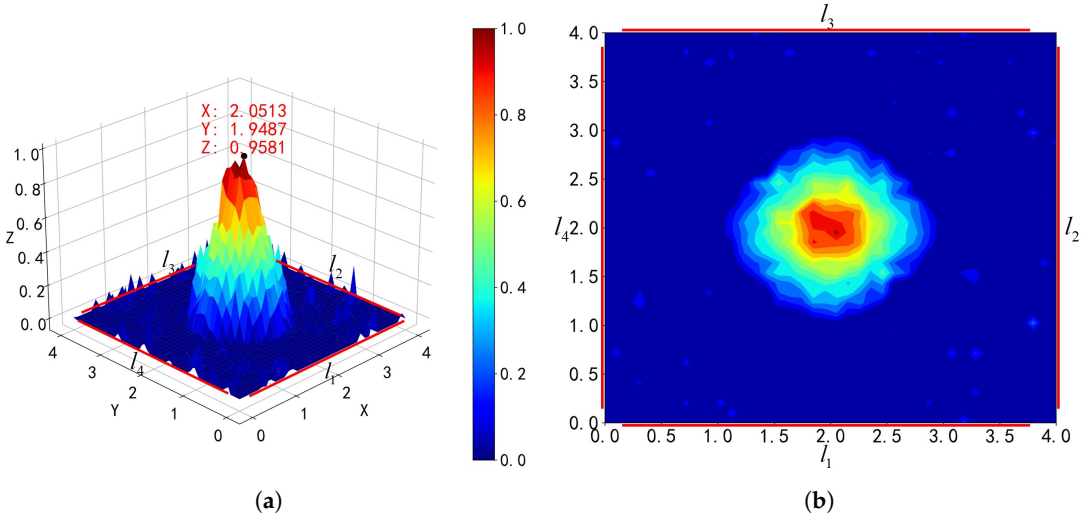

Figure 10. *Cont.*

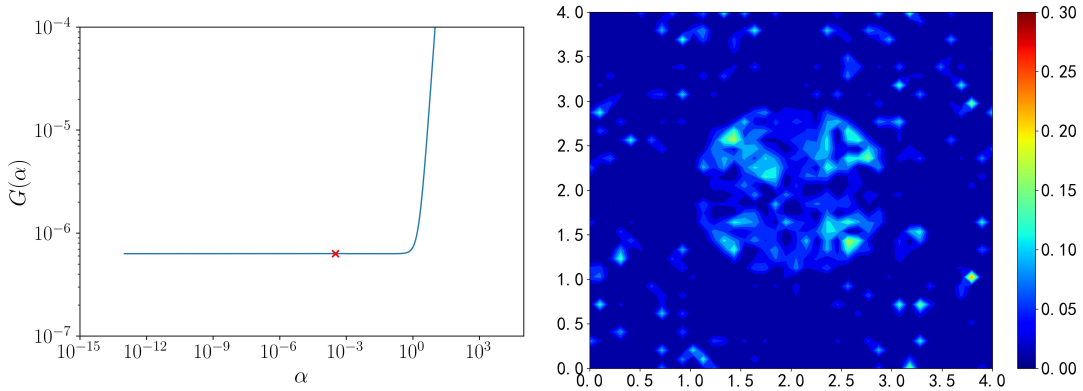

(**c**) (**d**)

Figure 10. When $\delta = 1\%$, the numerical inversion result of the source term was $f(x,y) = c^2\left[e^{-c_1 r_0} + e^{-c_1 r_1}\right] \cdot \left[2c_1c_2(x^2+y^2) - c_1^2\right]$. (**a**) The numerical inversion result of the source term; (**b**) the top view of the inversion results; (**c**) the regularization parameter selection, red × indicates the selected regularization parameter; and (**d**) the absolute value residual.

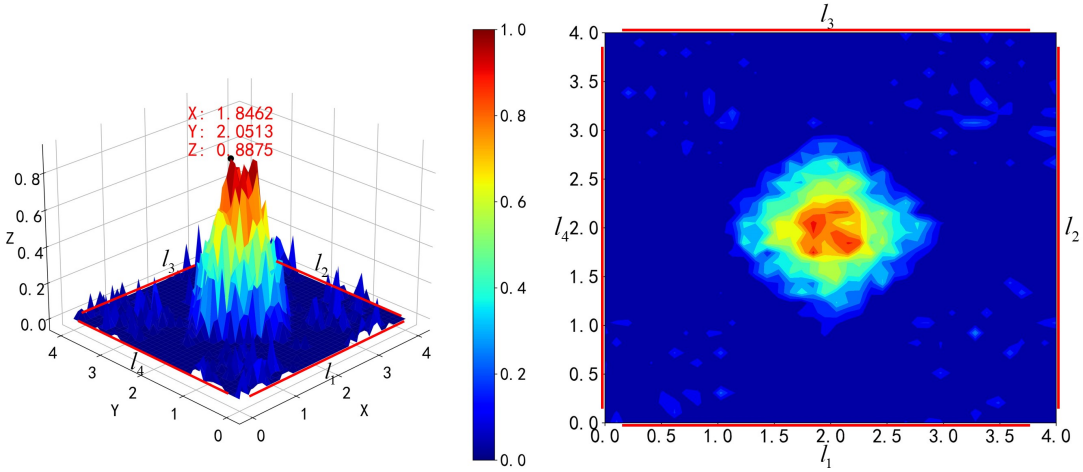

(**a**) (**b**)

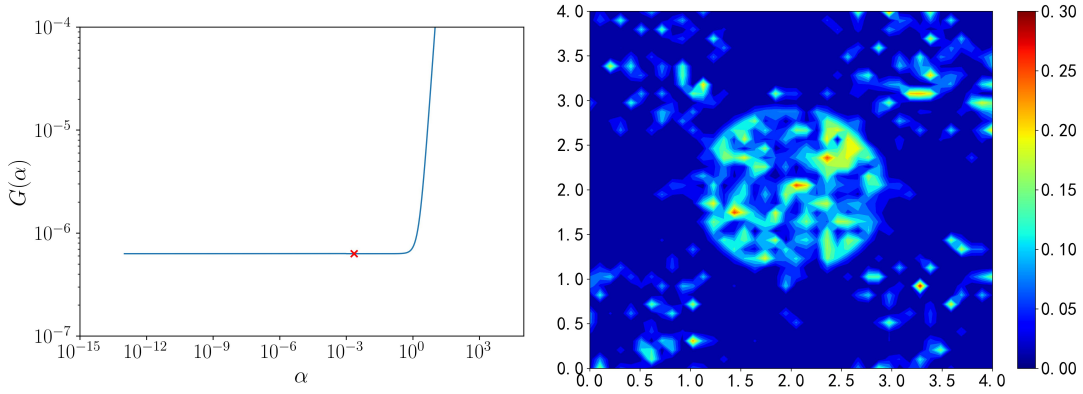

(**c**) (**d**)

Figure 11. When $\delta = 5\%$, the numerical inversion result of the source term was $f(x,y) = c^2\left[e^{-c_1 r_0} + e^{-c_1 r_1}\right] \cdot \left[2c_1c_2(x^2+y^2) - c_1^2\right]$. (**a**) The numerical inversion result of the source term; (**b**) the top view of the inversion results; (**c**) the regularization parameter selection, red × indicates the selected regularization parameter; and (**d**) the absolute value residual.

Table 3. In cases of multiple sources, the correlation coefficient changed with δ.

δ	e	α
0%	0.0310829	0.0000531
1%	0.1379291	0.0010352
5%	0.2233056	0.0038324

Numerical Example 3. *For cases where there are two source terms, we used the values of* $L_1 = 4$, $L_2 = 4$, $N_x = 40$, $N_y = 40$, *wave speed* $c = 0.1$, $T = 20$, *and source term function* $f(x,y) = c^2[e^{-c_1 r_0} + e^{-c_1 r_1}] \cdot [2c_1c_2(x^2+y^2) - c_1^2]$, *where* $(x_0, y_0) = (L_1/2, L_2/2)$, $(x_1, y_1) = (L_1/2, 3L_2/4)$, $c_1 = 4$, $c_2 = 10$, $r_0 = (x-x_0)^2 + (y-y_0)^2$, *and* $r_1 = (x-x_1)^2 + (y-y_1)^2$.

Figure 12a includes the source term function graph when the parameters were determined. Figures 13a, 14a, and 15a detail the numerical inversion results of the source term for the noise-free data, as well as the numerical inversion results of the source term with the addition of 1% and 5% noisy data, respectively. Different perturbations are listed in Table 4, along with the L^2 error results under the data condition and regularization parameter selection results.

Table 4. In cases of multiple sources, the correlation coefficient changed with δ.

δ	e	α
0%	0.5742650	0.0000131
1%	1.6943993	0.0003225
5%	3.9899033	0.0021990

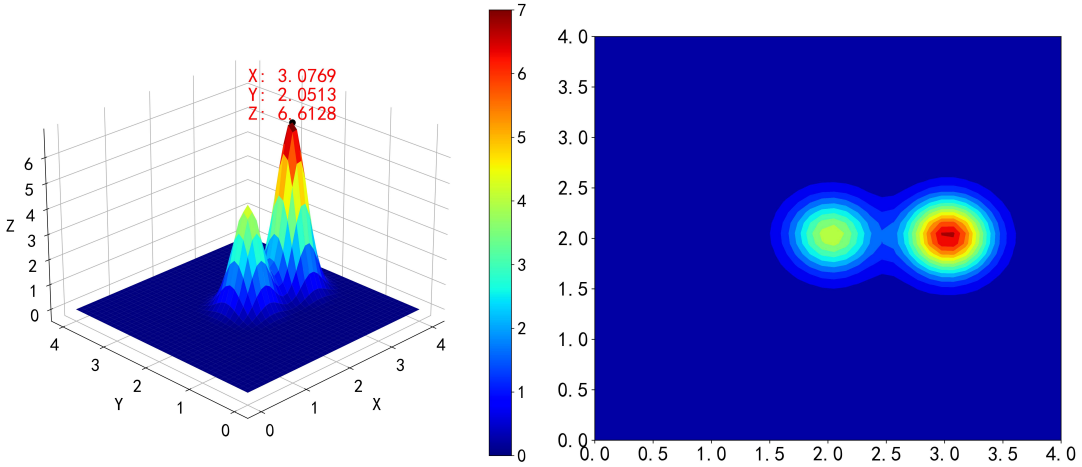

(**a**) (**b**)

Figure 12. The function graph of the source term $f(x,y) = c^2[e^{-c_1 r_0} + e^{-c_1 r_1}] \cdot [2c_1c_2(x^2+y^2) - c_1^2]$. (**a**) The source term function graph and (**b**) the top view of the source term function.

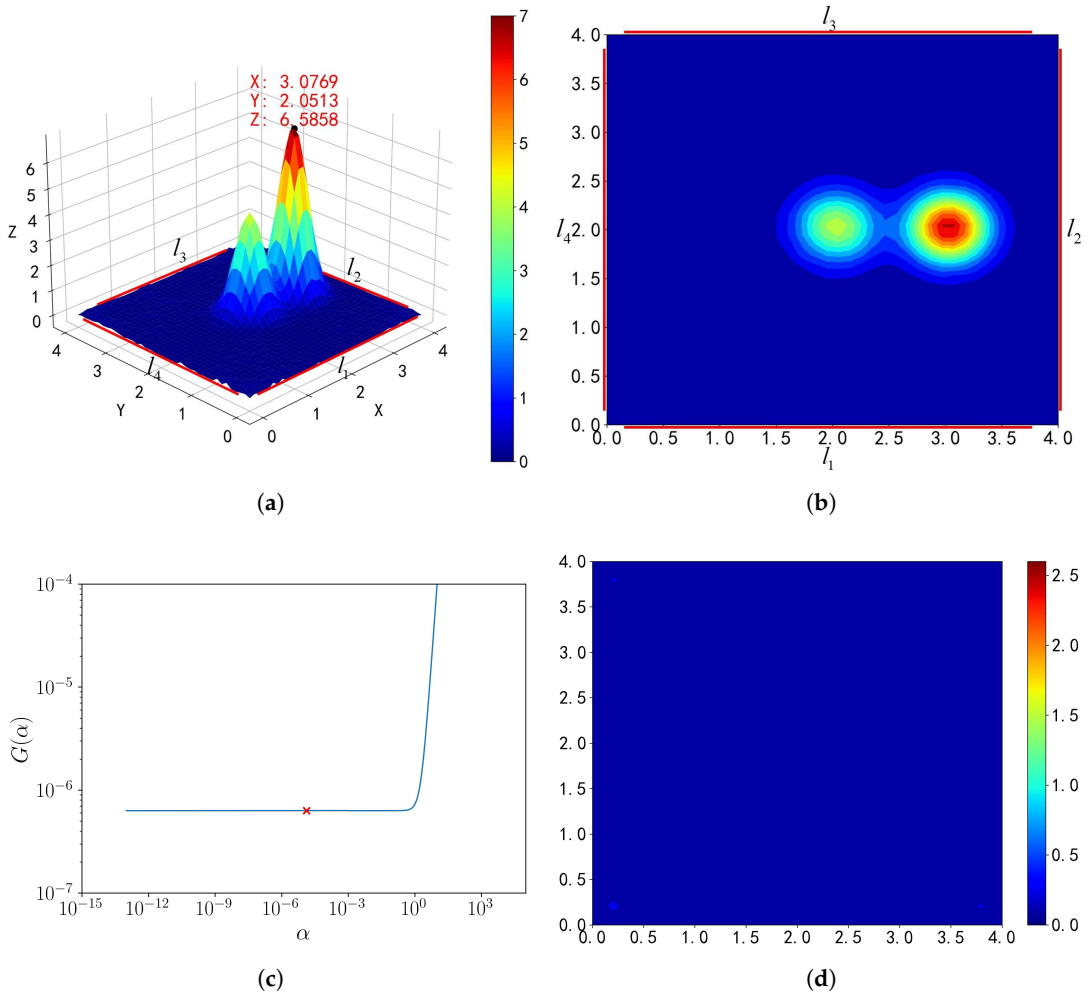

Figure 13. The numerical inversion result of the source term $f(x,y) = c^2\left[e^{-c_1 r_0} + e^{-c_1 r_1}\right] \cdot \left[2c_1c_2(x^2+y^2) - c_1^2\right]$. (**a**) The numerical inversion result of the source term; (**b**) the top view of the inversion results; (**c**) the regularization parameter selection, red × indicates the selected regularization parameter; and (**d**) the absolute value residual.

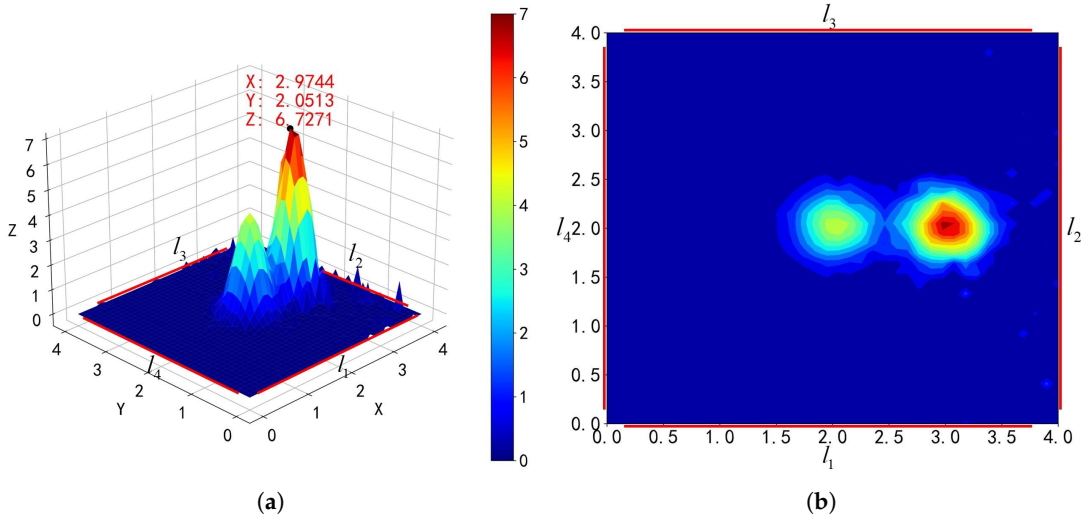

Figure 14. *Cont.*

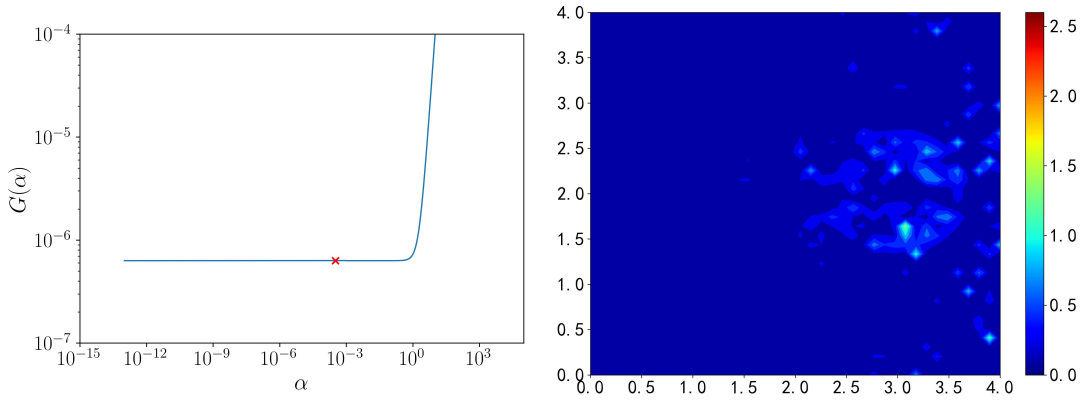

(**c**) (**d**)

Figure 14. When $\delta = 1\%$, the numerical inversion result of the source term was $f(x,y) = c^2\left[e^{-c_1 r_0} + e^{-c_1 r_1}\right] \cdot \left[2c_1c_2(x^2+y^2) - c_1^2\right]$. (**a**) The numerical inversion result of the source term; (**b**) the top view of the inversion results; (**c**) the regularization parameter selection, red × indicates the selected regularization parameter; and (**d**) the absolute value residual.

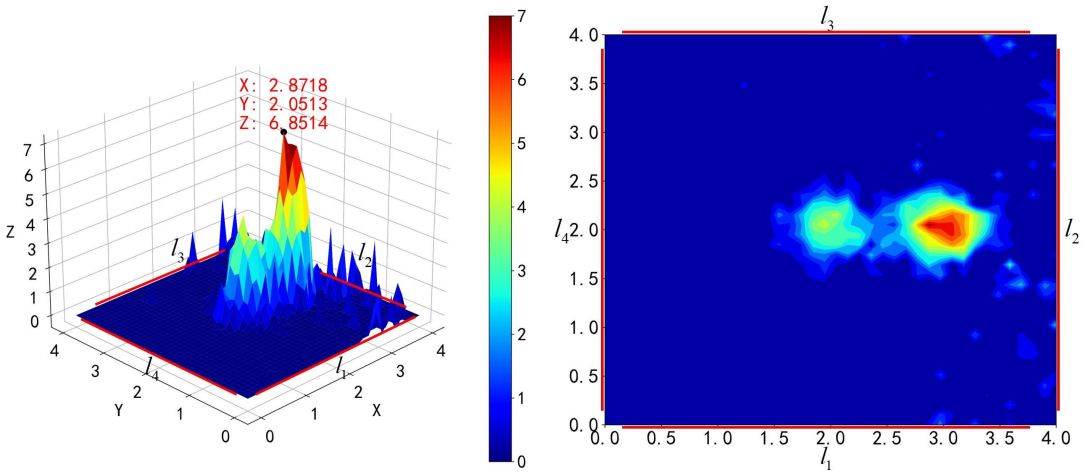

(**a**) (**b**)

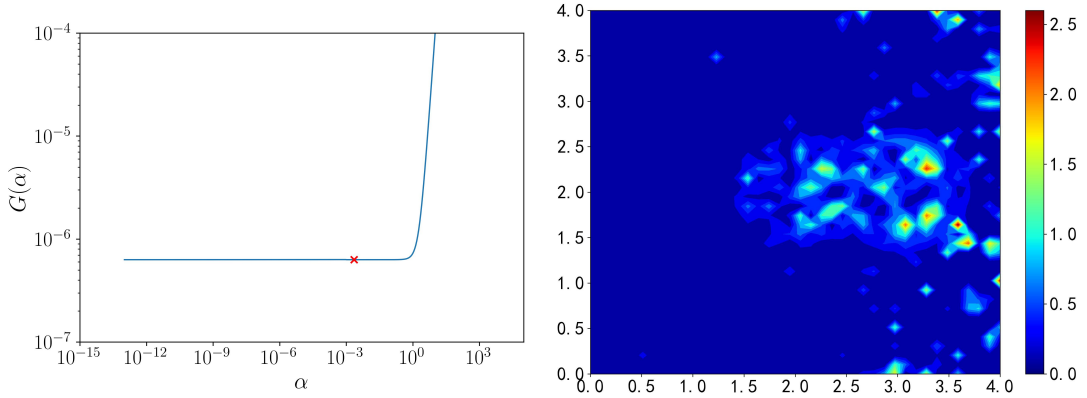

(**c**) (**d**)

Figure 15. When $\delta = 5\%$, the numerical inversion result of the source term was $f(x,y) = c^2\left[e^{-c_1 r_0} + e^{-c_1 r_1}\right] \cdot \left[2c_1c_2(x^2+y^2) - c_1^2\right]$. (**a**) The numerical inversion result of the source term; (**b**) the top view of the inversion results; (**c**) the regularization parameter selection, red × indicates the selected regularization parameter; and (**d**) the absolute value residual.

According to these three examples, the algorithm proposed in this paper has a better inversion effect on the source term when the data of the four sides are known. This applies to both single- and multiple-source types, with the algorithm more accurately inverting the shape and position of the source term function. In Numerical Example 1, the shape and position of the source term function can be roughly inverted even if the data on one side are missing, but when the source term function is inverted using the data on both sides, it is incomplete and has missing information. If we inverse the function with low smoothness, the shape and position of the source term can be roughly inverted, but the error is larger than that of the real source term.

Author Contributions: Formal analysis, L.S. and T.-Y.W.; methodology, T.-Y.W. and H.Z.; numerical example L.S.; writing—original draft preparation, L.S.; writing—review and editing, T.-Y.W. and H.Z.; supervision, T.-Y.W. All authors have read and agreed to the published version of the manuscript.

Funding: This research was funded by the NSFC grants 11971024 and 12061080.

Data Availability Statement: In terms of the data availability statement, it is affirmed that data are contained within the article, as the method of making DAS-type data is included in the article.

Conflicts of Interest: The authors declare no conflicts of interest.

Appendix A

The derivation of Equation (10) is as follows:

$$\begin{aligned} g(x, L_2, T) &= \int_x^{x_l} |u(\hat{x}, L_2, T)| d\hat{x} \\ &= \int_x^{x_l} \left| \int_0^{L_2} \int_0^{L_1} H(\hat{x}, L_2; \tilde{x}, \tilde{y}) f(\tilde{x}, \tilde{y})\, d\tilde{x} d\tilde{y} \right| d\hat{x} \\ &= \int_x^{x_l} \int_0^{L_2} \int_0^{L_1} H(\hat{x}, L_2; \tilde{x}, \tilde{y}) f(\tilde{x}, \tilde{y})\, d\tilde{x} d\tilde{y}\, d\hat{x} \\ &= \int_0^{L_2} \int_0^{L_1} \left(\int_x^{x_l} H(\hat{x}, L_2; \tilde{x}, \tilde{y})\, d\hat{x} \right) f(\tilde{x}, \tilde{y})\, d\tilde{x} d\tilde{y}. \end{aligned} \tag{A1}$$

For the derivation of Expressions $\hat{H}_{l_2}(x, y; \tilde{x}, \tilde{y})$, $\hat{H}_{l_3}(x, y; \tilde{x}, \tilde{y})$, and $\hat{H}_{l_4}(x, y; \tilde{x}, \tilde{y})$, we considered Edges l_1, and l_3 first, which integrate in the x direction. On Edge l_1, $y = 0$, and $x \in [dl, L_1 - dl]$; we obtained the following:

$$\hat{H}_{l_1}(x, 0; \tilde{x}, \tilde{y}) = \int_x^{x_l} H(\hat{x}, 0; \tilde{x}, \tilde{y})\, d\hat{x}. \tag{A2}$$

On Edge l_3, $y = L_2$, and $x \in [dl, L_1 - dl]$; we obtained the following:

$$\hat{H}_{l_3}(x, L_2; \tilde{x}, \tilde{y}) = \int_x^{x_l} H(\hat{x}, L_2; \tilde{x}, \tilde{y})\, d\hat{x}. \tag{A3}$$

Now, we simply need to consider the following:

$$\hat{H}_{l_{1,3}}(x, y; \tilde{x}, \tilde{y}) = \int_x^{x_l} H(\hat{x}, y; \tilde{x}, \tilde{y})\, d\hat{x} = \frac{1}{2\pi c} \int_x^{x_l} \frac{I_{(\hat{x}-\tilde{x})^2 + (y-\tilde{y})^2 < c^2 T^2}}{\sqrt{c^2 T^2 - (\hat{x} - \tilde{x})^2 - (y - \tilde{y})^2}}\, d\hat{x} \tag{A4}$$

since $\hat{H}_{l_1}(x, 0; \tilde{x}, \tilde{y}) = \hat{H}_{l_{1,3}}(x, 0; \tilde{x}, \tilde{y})$, and $\hat{H}_{l_3}(x, L_2; \tilde{x}, \tilde{y}) = \hat{H}_{l_{1,3}}(x, L_2; \tilde{x}, \tilde{y})$.

For a fixed $(\tilde{x}, \tilde{y})$, there are the following four cases:

(1) $I_1 := \{(x, y) | (x - \tilde{x})^2 + (y - \tilde{y})^2 \geq c^2 T^2, (x_l - \tilde{x})^2 + (y - \tilde{y})^2 \geq c^2 T^2\}$. For $(x, y) \in I_1$, any $\hat{x} \in (x, x_l)$, and $H(\hat{x}, y; \tilde{x}, \tilde{y}) = 0$, we have

$$\hat{H}_{l_{1,3}}(x, y; \tilde{x}, \tilde{y}) = 0. \tag{A5}$$

(2) $I_2 := \{(x,y)|(x-\tilde{x})^2+(y-\tilde{y})^2 < c^2T^2, (x_l-\tilde{x})^2+(y-\tilde{y})^2 > c^2T^2\}$. For $(x,y) \in I_2$, there exists $x_a = \tilde{x} + \sqrt{c^2T^2-(y-\tilde{y})^2} \in [x, x_l]$ such that $(x_a-\tilde{x})^2+(y-\tilde{y})^2 = c^2T^2$. As such, for $\hat{x} \in (x_a, x_l)$ and $H(\hat{x}, y; \tilde{x}, \tilde{y}) = 0$, we have

$$\begin{aligned}
\hat{H}_{l_{1,3}}(x,y;\tilde{x},\tilde{y}) &= \int_x^{x_l} H(\hat{x},y;\tilde{x},\tilde{y})\,d\hat{x} \\
&= \int_x^{x_a} H(\hat{x},y;\tilde{x},\tilde{y})\,d\hat{x} \\
&= \frac{1}{2\pi c}\int_x^{x_a} \frac{1}{\sqrt{c^2T^2-(\hat{x}-\tilde{x})^2-(y-\tilde{y})^2}}\,d\hat{x} \\
&= \frac{1}{2\pi c}\left(\arcsin\frac{x_a-\tilde{x}}{\sqrt{c^2T^2-(y-\tilde{y})^2}} - \arcsin\frac{x-\tilde{x}}{\sqrt{c^2T^2-(y-\tilde{y})^2}}\right) \\
&= \frac{1}{2\pi c}\left(\frac{\pi}{2} - \arcsin\frac{x-\tilde{x}}{\sqrt{c^2T^2-(y-\tilde{y})^2}}\right).
\end{aligned} \tag{A6}$$

(3) $I_3 := \{(x,y)|(x-\tilde{x})^2+(y-\tilde{y})^2 \geq c^2T^2, (x_l-\tilde{x})^2+(y-\tilde{y})^2 < c^2T^2\}$. For $(x,y) \in I_3$, there exists $x_b = \tilde{x} - \sqrt{c^2T^2-(y-\tilde{y})^2} \in [x, x_l]$ such that $(x_b-\tilde{x})^2+(y-\tilde{y})^2 = c^2T^2$. As such, for $\hat{x} \in (x, x_b)$ and $H(\hat{x}, y; \tilde{x}, \tilde{y}) = 0$, we have

$$\begin{aligned}
\hat{H}_{l_{1,3}}(x,y;\tilde{x},\tilde{y}) &= \int_x^{x_l} H(\hat{x},y;\tilde{x},\tilde{y})\,d\hat{x} \\
&= \int_{x_b}^{x_l} H(\hat{x},y;\tilde{x},\tilde{y})\,d\hat{x} \\
&= \frac{1}{2\pi c}\int_{x_b}^{x_l} \frac{1}{\sqrt{c^2T^2-(\hat{x}-\tilde{x})^2-(y-\tilde{y})^2}}\,d\hat{x} \\
&= \frac{1}{2\pi c}\left(\arcsin\frac{x_l-\tilde{x}}{\sqrt{c^2T^2-(y-\tilde{y})^2}} - \arcsin\frac{x_b-\tilde{x}}{\sqrt{c^2T^2-(y-\tilde{y})^2}}\right) \\
&= \frac{1}{2\pi c}\left(\arcsin\frac{x+dl-\tilde{x}}{\sqrt{c^2T^2-(y-\tilde{y})^2}} + \frac{\pi}{2}\right).
\end{aligned} \tag{A7}$$

(4) $I_4 := \{(x,y)|(x-\tilde{x})^2+(y-\tilde{y})^2 < c^2T^2, (x_l-\tilde{x})^2+(y-\tilde{y})^2 < c^2T^2\}$. For $(x,y) \in I_4$, any $\hat{x} \in (x, x_l)$, and $\hat{H}_{l_{1,3}}(x,y;\tilde{x},\tilde{y}) > 0$, we have

$$\begin{aligned}
\hat{H}_{l_{1,3}}(x,y;\tilde{x},\tilde{y}) &= \int_x^{x_l} H(\hat{x},y;\tilde{x},\tilde{y})\,d\hat{x} \\
&= \frac{1}{2\pi c}\int_x^{x_l} \frac{1}{\sqrt{c^2T^2-(\hat{x}-\tilde{x})^2-(y-\tilde{y})^2}}\,d\hat{x} \\
&= \frac{1}{2\pi c}\left(\arcsin\frac{x+dl-\tilde{x}}{\sqrt{c^2T^2-(y-\tilde{y})^2}} - \arcsin\frac{x-\tilde{x}}{\sqrt{c^2T^2-(y-\tilde{y})^2}}\right).
\end{aligned} \tag{A8}$$

According to Formulas (A5)–(A8), for the given $(\tilde{x}, \tilde{y})$, we can obtain

$$\hat{H}_{l_{1,3}}(x,y;\tilde{x},\tilde{y}) = \begin{cases} 0, & (x,y) \in I_1, \\ \frac{1}{2\pi c}\left(\frac{\pi}{2} - \arcsin\frac{x-\tilde{x}}{\sqrt{c^2T^2-(y-\tilde{y})^2}}\right), & (x,y) \in I_2, \\ \frac{1}{2\pi c}\left(\arcsin\frac{x+dl-\tilde{x}}{\sqrt{c^2T^2-(y-\tilde{y})^2}} + \frac{\pi}{2}\right), & (x,y) \in I_3, \\ \frac{1}{2\pi c}\left(\arcsin\frac{x+dl-\tilde{x}}{\sqrt{c^2T^2-(y-\tilde{y})^2}} - \arcsin\frac{x-\tilde{x}}{\sqrt{c^2T^2-(y-\tilde{y})^2}}\right), & (x,y) \in I_4. \end{cases} \tag{A9}$$

Similarly, let $y_l = y + dl$. On Edge l_2, where $x = L_1$, and $y \in [dl, L_2 - dl]$, we obtain the following:

$$\hat{H}_{l_2}(L_1, y; \tilde{x}, \tilde{y}) = \int_y^{y_l} H(L_1, \hat{y}; \tilde{x}, \tilde{y})\, d\hat{y}. \tag{A10}$$

On Edge l_4, where $x = 0$, and $y \in [dl, L_2 - dl]$, we obtain the following:

$$\hat{H}_{l_4}(0, y; \tilde{x}, \tilde{y}) = \int_y^{y_l} H(0, \hat{y}; \tilde{x}, \tilde{y})\, d\hat{y}. \tag{A11}$$

Now, we simply need to consider the following:

$$\hat{H}_{l_{2,4}}(x, y; \tilde{x}, \tilde{y}) = \int_y^{y_l} H(x, \hat{y}; \tilde{x}, \tilde{y})\, d\hat{y} = \frac{1}{2\pi c} \int_y^{y_l} \frac{I_{(x-\tilde{x})^2 + (\hat{y}-\tilde{y})^2 < c^2T^2}}{\sqrt{c^2T^2 - (x-\tilde{x})^2 - (\hat{y}-\tilde{y})^2}}\, d\hat{y} \tag{A12}$$

since $\hat{H}_{l_2}(L_1, y; \tilde{x}, \tilde{y}) = \hat{H}_{l_{2,4}}(L_1, y; \tilde{x}, \tilde{y})$ and $\hat{H}_{l_4}(0, y; \tilde{x}, \tilde{y}) = \hat{H}_{l_{2,4}}(0, y; \tilde{x}, \tilde{y})$.

There are also the following four cases:

$$I_5 = \left\{(x, y) | (x-\tilde{x})^2 + (y_l - \tilde{y})^2 \geq c^2T^2, (x-\tilde{x})^2 + (y_l - \tilde{y})^2 \geq c^2T^2\right\}, \tag{A13}$$

$$I_6 = \left\{(x, y) | (x-\tilde{x})^2 + (y_l - \tilde{y})^2 < c^2T^2, (x-\tilde{x})^2 + (y_l - \tilde{y})^2 > c^2T^2\right\}, \tag{A14}$$

$$I_7 = \left\{(x, y) | (x-\tilde{x})^2 + (y_l - \tilde{y})^2 \geq c^2T^2, (x-\tilde{x})^2 + (y_l - \tilde{y})^2 < c^2T^2\right\}, \tag{A15}$$

$$I_8 = \left\{(x, y) | (x-\tilde{x})^2 + (y_l - \tilde{y})^2 < c^2T^2, (x-\tilde{x})^2 + (y_l - \tilde{y})^2 < c^2T^2\right\}. \tag{A16}$$

From (A9), for a fixed $(\tilde{x}, \tilde{y})$, we have

$$\hat{H}_{l_{2,4}}(x, y; \tilde{x}, \tilde{y}) = \begin{cases} 0, & (x, y) \in I_5, \\ \frac{1}{2\pi c}\left(\frac{\pi}{2} - \arcsin \frac{y-\tilde{y}}{\sqrt{c^2T^2-(x-\tilde{x})^2}}\right), & (x, y) \in I_6, \\ \frac{1}{2\pi c}\left(\arcsin \frac{y+dl-\tilde{y}}{\sqrt{c^2T^2-(x-\tilde{x})^2}} + \frac{\pi}{2}\right), & (x, y) \in I_7, \\ \frac{1}{2\pi c}\left(\arcsin \frac{y+dl-\tilde{y}}{\sqrt{c^2T^2-(x-\tilde{x})^2}} - \arcsin \frac{y-\tilde{y}}{\sqrt{c^2T^2-(x-\tilde{x})^2}}\right), & (x, y) \in I_8. \end{cases} \tag{A17}$$

References

1. Zhan, Z. Distributed acoustic sensing turns fiber-optic cables into sensitive seismic antennas. *Seismol. Res. Lett.* **2020**, *91*, 1–15. [CrossRef]. [CrossRef]
2. Fernández-Ruiz, M.; Soto, M.; Williams, E.; Martín-López, S.; Zhan, Z.; González-Herráez, M.; Martins, H. Distributed acoustic sensing for seismic activity monitoring. *APL Photonics* **2020**, *5*, 030901. [CrossRef]. [CrossRef]
3. Willis, M.; Barfoot, D.A.; Ellmauthaler, A.; Wu, X.; Barrios, O.; Erdemir, C.; Shaw, S.; Quinn, D. Quantitative quality of distributed acoustic sensing vertical seismic profile data. *Geophysics* **2016**, *35*, 605–609. [CrossRef]. [CrossRef]
4. Shang, Y.; Sun, M.; Wang, C.; Yang, J.; Du, Y.; Yi, J.; Zhao, W.; Wang, Y.; Zhao, Y.; Ni, J. Research Progress in Distributed Acoustic Sensing Techniques. *Sensors* **2022**, *22*, 6060. [CrossRef]. [CrossRef] [PubMed]
5. Asiri, S.; Zayane-Aissa, C.; Laleg-Kirati, T. An Adaptive Observer-Based Algorithm for Solving Inverse Source Problem for the Wave Equation. *Math. Probl. Eng.* **2015**, *2015*, 796539. [CrossRef]. [CrossRef]
6. Sattari Shajari, P.; Shidfar, A. Application of weighted homotopy analysis method to solve an inverse source problem for wave equation. *Inverse Probl. Sci. Eng.* **2019**, *27*, 61–88. [CrossRef]. [CrossRef]
7. Hu, G.h.; Kian, Y.; Zhao, Y. Uniqueness to some inverse source problems for the wave equation in unbounded domains. *Acta Math. Appl. Sin. Engl. Ser.* **2020**, *36*, 134–150. [CrossRef]. [CrossRef]
8. Liu, C.S.; Qiu, L.; Wang, F. Nonlinear wave inverse source problem solved by a method of m-order homogenization functions. *Appl. Math. Lett.* **2019**, *91*, 90–96. [CrossRef]. [CrossRef]
9. Arumugam, D.; Prakash, P.; Nieto, J. Optimization method for identifying the source term in an inverse wave equation. *Electron. J. Differ. Equ.* **2017**, *2017*, 1–15.
10. Chorfi, S.E.; El Guermai, G.; Maniar, L.; Zouhair, W. Identification of source terms in wave equation with dynamic boundary conditions. *Math. Methods Appl. Sci.* **2023**, *46*, 911–929. [CrossRef]. [CrossRef]
11. Cannon, J.; DuChateau, P. An inverse problem for an unknown source term in a wave equation. *SIAM J. Appl. Math.* **1983**, *43*, 553–564. [CrossRef]. [CrossRef]

12. Tikhonov, A.N.; Goncharsky, A.V.; Stepanov, V.V.; Yagola, A.G. *Numerical Methods for the Solution of Ill-Posed Problems*; Kluwer Academic Publishers Group: Dordrecht, The Netherlands, 1995. [CrossRef].
13. Borisov, D.; Gao, F.; Williamson, P.; Tromp, J. Application of 2D full-waveform inversion on exploration land data. *Geophysics* **2020**, *85*, R75–R86. [CrossRef]. [CrossRef]
14. Xiao, T.; Yu, S.; Wang, Y. *Numerical solutions to inverse problems*; Science Press: Beijing, China, 2003.
15. Evans, L.C. *Partial differential Equations*; American Mathematical Society: Providence, RI, USA, 2022; Volume 19.
16. El Badia, A.; Ha-Duong, T. Determination of point wave sources by boundary measurements. *Inverse Probl.* **2001**, *17*, 1127. [CrossRef]. [CrossRef]
17. Lukas, M.A. Robust generalized cross-validation for choosing the regularization parameter. *Inverse Probl.* **2006**, *22*, 1883. [CrossRef]. [CrossRef]